Journal of Structural Geology 37 (2012) 89–104

Contents lists available at SciVerse ScienceDirect

Journal of Structural Geology

journal homepage: www.elsevier.com/locate/jsg

Extreme ductile deformation of fine-grained salt by coupled solution-precipitation creep and microcracking: Microstructural evidence from perennial Zechstein sequence (Neuhof salt mine, Germany)

Prokop Závada [a,*], Guillaume Desbois [b], Alexander Schwedt [c], Ondrej Lexa [d], Janos L. Urai [b]

[a] Institute of Geophysics ASCR, v.v.i.; Boční II/1401, 141 31 Prague, Czech Republic
[b] Structural Geology, Tectonics and Geomechanics, RWTH Aachen University, Lochnerstr. 4-20, D-52056 Aachen, Germany
[c] Gemeinschaftslabor für Elektronenmikroskopie, RWTH Aachen, Ahornstr. 55, 52074 Aachen, Germany
[d] Institute of Petrology and Structural Geology, Charles University, Albertov 6, 128 43 Prague, Czech Republic

ARTICLE INFO

Article history:
Received 4 March 2011
Received in revised form
3 January 2012
Accepted 24 January 2012
Available online 1 February 2012

Keywords:
Rock salt
Solution-precipitation creep
Microcracking
Griffith crack
Fluid inclusion trails
Perennial lake
Salt rafts

ABSTRACT

Microstructural study revealed that the ductile flow of intensely folded fine-grained salt exposed in an underground mine (Zechstein-Werra salt sequence, Neuhof mine, Germany) was accommodated by coupled activity of solution-precipitation (SP) creep and microcracking of the halite grains. The grain cores of the halite aggregates contain remnants of sedimentary microstructures with straight and chevron shaped fluid inclusion trails (FITs) and are surrounded by two concentric mantles reflecting different events of salt precipitation. Numerous intra-granular or transgranular microcracks originate at the tips of FITs and propagate preferentially along the interface between sedimentary cores and the surrounding mantle of reprecipitated halite. These microcracks are interpreted as tensional Griffith cracks. Microcracks starting at grain boundary triple junctions or grain boundary ledges form due to stress concentrations generated by grain boundary sliding (GBS). Solid or fluid inclusions frequently alter the course of the propagating microcracks or the cracks terminate at these inclusions. Because the inner mantle containing the microcracks is corroded and is surrounded by microcrack-free outer mantle, microcracking is interpreted to reflect transient failure of the aggregate. Microcracking is argued to play a fundamental role in the continuation and enhancement of the SP–GBS creep during halokinesis of the Werra salt, because the transgranular cracks (1) provide the ingress of additional fluid in the grain boundary network when cross-cutting the FITs and (2) decrease grain size by splitting the grains. More over, the ingress of additional fluids into grain boundaries is also provided by non-conservative grain boundary migration that advanced into FITs bearing cores of grains. Described readjustments of the microstructure and mechanical and chemical feedbacks for the grain boundary diffusion flow in halite-brine system are proposed to be comparable to other rock-fluid or rock-melt aggregates deforming by the grain boundary sliding (GBS) coupled deformation mechanisms.

1. Introduction

The metamorphosis, deformation style and associated deformation mechanisms of rock salt in the entire diapiric system can be qualitatively compared with the deformation style of silicate rocks during orogenic exhumation (Talbot, 1998). Since rock salt consists primarily of monophase polycrystalline halite, the analysis of its deformation style and associated deformation mechanisms is relatively simple in comparison with silicate rocks, which mainly consist of several phases (polyphase rocks) that interact mechanically and chemically (Handy, 1994; Schulmann et al., 2008b). Relatively weak bonding strength of the atoms in the halite lattice relative to silicate minerals (Goldich, 1938) and a significant amount of fluid (brine) in the grain boundaries (e.g. Urai et al., 1986; Schoenherr et al., 2010) makes the recrystallization of halite much easier in comparison to silicate minerals. The investigation of deformed polycrystalline halite aggregates therefore helps understanding the role of deformation mechanisms that control deformation of rocks in general (e.g. Poirier, 1985; Drury and Urai, 1990). Besides the property of rock salt as a convenient analog for deformed complex lithologies, the analysis of its rheological properties is fundamental for understanding salt tectonics and

* Corresponding author. Tel.: +42 267 103 313; fax: +42 272 761 549.
E-mail address: zavada@ig.cas.cz (P. Závada).

0191-8141/$ – see front matter © 2012 Elsevier Ltd. All rights reserved.
doi:10.1016/j.jsg.2012.01.024

tackling drilling problems in salt and oil bearing sedimentary systems and engineering tasks regarding the design and maintenance of gas and radioactive waste storage caverns (Langer, 1993; Berest et al., 2005; Lux, 2005; Perry, 2005). Flow of rock salt also strongly influences the evolution and architecture of deforming salt-bearing sedimentary basins that contain the gas and oil deposits (Rowan et al., 1999; Hudec and Jackson, 2007; Littke et al., 2008).

Although the time-scales for extrusion of salt rocks from their source layers through diapirs and salt fountains on the Earth surface and exhumation of silicate rocks from orogenic roots to upper-crustal levels differs in the range of about 4–5 orders of magnitude (10^{3-4} yrs for salt diapirs, 10^{7-8} yrs for orogens; Talbot, 1998; Talbot and Aftabi, 2004; Culshaw et al., 2006; Schulmann et al., 2008a), the resulting fabrics and identified deformation mechanisms appear similar. During their exhumation, both, rock salt and silicate rocks undergo dynamic recrystallization and deform by mechanisms that are strongly controlled by intergranular fluid phase. The fluids accelerate the transfer of matter through diffusion and enhance the rate of grain boundary migration - GBM (Jaoul et al., 1984; Schenk and Urai, 2005; Schenk et al., 2006; Schmatz and Urai, 2010) and promote activity of grain-size sensitive diffusion creep (Tullis and Yund, 1991; Hirth and Kohlstedt, 1995; Závada et al., 2007; Schulmann et al., 2008b; Rybacki et al., 2010) or solution-precipitation accommodated grain boundary sliding (Spiers et al., 1990; Kenis et al., 2005; Ter Heege et al., 2005; Schléder, 2006; Schléder and Urai, 2007; Schoenherr et al., 2010; Desbois et al., 2010).

Schléder (2006), Schoenherr et al. (2010) and Desbois et al. (2010) summarized the microstructural mechanisms that control creep of salt in the entire salt diapiric system from the "source layer", to the salt "stock/wall" and extrusive "glacier/fountain" (Talbot and Jackson, 1987; Talbot, 1998), respectively. Although the relative contribution and activity of these mechanisms can strongly vary in different layers of salt, the general scheme is as follows: high differential flow stresses in the source layer and salt stock/wall are responsible for combined grain boundary migration (GBM) and sub-grain rotation (SGR) producing dynamically recrystallized fabric, while extrusive salts that are associated with relatively low flow stresses (Schléder and Urai, 2007) reveal dominant activity of solution-precipitation (SP) creep coupled with grain boundary sliding (GBS) typical for the fine-grained fabric and elongated grains (Desbois et al., 2010). An exception from this simplified summary of identified deformation mechanisms in rock salt is represented by the Zechstein salt in the Werra and Fulda basin, Neuhof, Germany, where the intense folding of a narrow fine-grained perennial-lake sequence was accommodated by SP creep and GBS (Schléder et al., 2008).

In contrast to the crystal-plastic deformation mechanisms and SP creep that accommodate relatively slow ductile deformation of rock salt in nature, in laboratory experiments conducted at relatively low temperatures, high differential stresses (and high strain rates) and low confining pressures (e.g. Peach et al., 2001; Urai and Spiers, 2007; Niemeijer et al., 2010) rock salt fails in a brittle manner (Schulze et al., 2001; Popp et al., 2001). This mechanical failure is manifested by opening of inter- and intra-granular microfractures (dilatancy), which can finally lead to comminution of grains and transitions from ductile and semibrittle to cataclastic deformation and unstable stick-slip faulting (Niemeijer et al., 2010). The dilatancy can be also induced by high pore fluid pressures to produce fluid filled microfractures parallel with the maximum compressive stress direction (Hubbert and Rubey, 1959; Price and Cosgrove, 1990), as described for numerous creep experiments with melt bearing granular aggregates (Daines and Kohlstedt, 1997; Gleason et al., 1999; Rosenberg, 2001; Holtzman et al., 2003). Similar dilated microstructures were described for Ara rock salt (Oman) that was penetrated by oil from adjacent reservoirs, where oil pressure was close to lithostatic (Schoenherr et al., 2007). Another example of fluid induced dilatancy is the halite veining in the Werra rock salt from the Neuhof mine (Schléder et al., 2008). However, the interplay of different deformation mechanisms including microcracking at slow strain rates typical for flow of rock salt in the diapiric systems is poorly known.

The microstructural analysis of rock salt is facilitated by combination of several techniques such as gamma-irradiation, etching of thin sections, textural analysis of digitized polycrystalline aggregates (Lexa et al., 2005; Desbois et al., 2010) and EBSD (Electron Back Scattered Diffraction) analysis of the crystallographic preferred orientation. Gamma-irradiation induces damage on atomic scale in the halite lattice, which can decorate halite microstructure in blue (Urai et al., 1987; Celma and Donker, 1996; Schléder and Urai, 2007; Schoenherr et al., 2010). The physical basis of the blue decoration of halite microstructures is the production of F-center defects during irradiation, which aggregate into sodium colloids, while H-centers, representing the Cl_2 molecules, remain white (van Opbroek and den Hartog, 1985; Celma and Donker, 1994). The intensity of the blue coloration is a function of sodium colloids concentration at solid-solution impurities and crystal-defect sites (Jain–Lidiard model). The gamma-irradiation together with the etching technique reveals a range of microstructures characterizing the different deformation and fluid transport mechanisms in rock salt; syn-sedimentary cores of grains, growth bands, sub-grains, dissolution-precipitation features, etc. (Przibram, 1954; Urai et al., 1986, 1987, 2008; Schléder and Urai, 2007; Schléder et al., 2008; Schoenherr et al., 2010; Desbois et al., 2010). Although high gamma-irradiation doses can induce solid-state deformation and migration of fluid inclusions (Celma and Donker, 1994), these effects are minor at relatively low gamma-irradiation doses (as used in this contribution) and can be distinguished from the microstructures produced by natural deformation of the investigated specimens (Anthony and Cline, 1973; Holdoway, 1973; Celma and Donker, 1994; Schléder et al., 2007).

This contribution focuses on the details of the Werra rock salt microstructure previously investigated by Schléder et al. (2008) to give detailed description of microstructures and emphasize the role of microcracking for the enhancement of SP creep coupled with GBS. Our findings are based on detailed analysis of thin sections prepared from gamma-irradiated specimens, EBSD (Electron Back Scattered Diffraction) mapping of the thin sections, orientation measurements of microcracks using universal stage and comparison of their orientation with crystallographic orientation of corresponding grains.

2. Geological setting

The investigated rock salt was sampled by horizontal core-drilling in the Neuhof-Ellers salt mine (Fig. 1a) and represents the Upper Werra rock salt, a 0.3–2 m thick layer within the 300 m thick Zechstein (Z1) salt sequence, which was deposited unconformably on the top of Permian sediments at the southern margin of the Permian Zechstein basin (Lockhorst, 1998). The Z1 layer is overlain by a 350 m thick pile of siliciclastic Buntsandstein sediments. Detailed descriptions of the geological situation in the area of interest are given by Leammlen (1970), Roth (1957), Käding and Sessler (1994) and Beer (1996). In contrast to the overlying Z1 salt beds, which are undeformed, the Upper Werra (and to a lesser degree the underlying Hessen potash seam) are extensively folded (Fig. 1b). The Upper Werra rock salt reveals mechanical decoupling at its base and isoclinal folds with fold planes inclined at more than 45°, and NE vergence. The mobilization of this narrow salt unit was

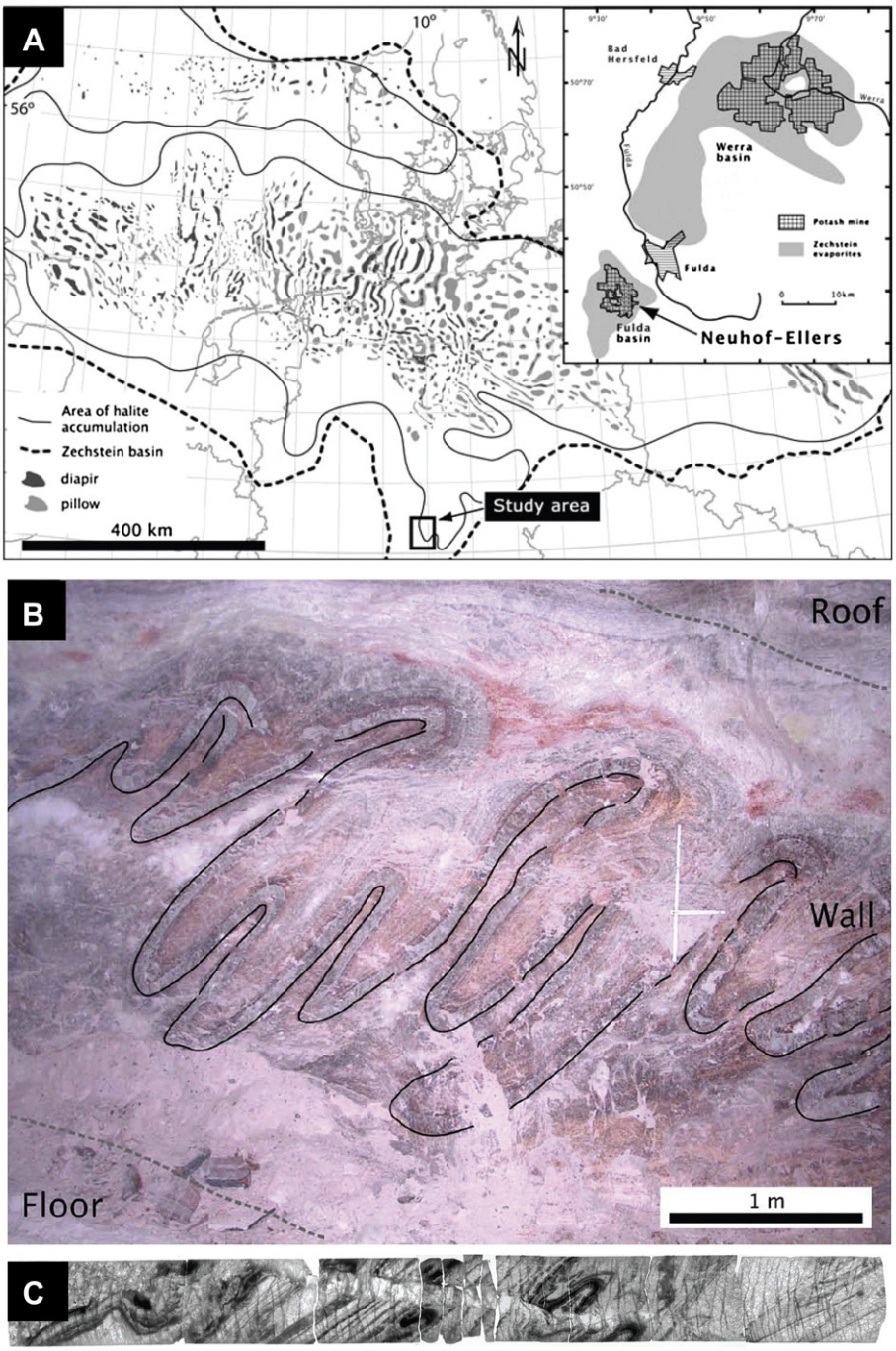

Fig. 1. (a) Map indicating the location of the study area in the Zechstein basin (after Roth, 1957; Lockhorst, 1998). (b) Photograph of the folded Werra rock salt sequence at outcrop scale in the Neuhof-Ellers salt mine. (c) Scanned surface of the investigated horizontal borehole (c). Figures taken from Schléder et al. (2008).

attributed to differential loading during Jurassic and Cretaceous (Hoppe, 1960; Schléder et al., 2007).

The investigated Upper Werra rock salt in the horizontal borehole (Fig. 1c) is cross-cut by several halite filled veins. These veins were suggested to develop by hydrofracturing of the sequence, and drained the fluids generated by mineral transformations in the underlying salt layers (Schléder et al., 2007).

3. Methods

Slabs cut perpendicular to the axial planes of the folds were prepared from a core in the Upper Werra salt sequence. The slabs were gamma-irradiated at 100 °C, with a dose rate of 1–4 kGy/h to a total dose of 4 MGy, which was followed by thin section preparation from the slabs (Schléder and Urai, 2005). Microstructure observations under optical microscope in transmitted light were performed on 10 different gamma-irradiated thin sections.

The gamma-irradiated rock salt aggregate in one thin section was digitized in ArcView GIS environment using the extension Poly and statistically evaluated using the PolyLX toolbox in MatLab™ (Lexa et al., 2005). The textural analysis comprised grain-size statistics of the grains, the area fraction of non-recrystallized parts of the grains and directional analysis of long axes of grains and traces of fluid inclusions and healed microcracks in one thin

section. To reveal the crystal orientation pattern, we employed EBSD analysis (Electron Back Scattered Diffraction) on a JEOL JSM 7000F SEM (Gemeinschaftslabor für Elektronenmikroskopie, RWTH Aachen) with an EDAX-TSL DigiView III detector, equipped with OIM Data Collection/OIM Analysis (version 5.2) software. The pattern was acquired at an acceleration voltage of 25 kV, probe current ~15 nA and working distance 29 mm. A thin section of sample 1-9b was scanned in an area of about 3.2 cm × 4.4 cm as combo scan measuring 72 single fields at a magnification of 33× with a step size of 25 microns and an indexing rate of about 82%. A light clean-up was applied in order to remove erroneous single-pixel results using a single-iteration of the grain-dilation algorithm implemented in OIM Analysis assuming a grain tolerance angle of 5° and a minimum grain size of two pixels. The substructures of selected grains using misorientation profiles were analyzed in another thin section (sample 1-18b) from correlation of the 7.2 mm × 5.6 mm EBSD map and the corresponding gamma-irradiated microstructure. The latter EBSD map was assembled from 27 single fields collected at 200× magnification, a step size of 10 microns and indexing rate of 97%.

In the next step the orientations of the planar fluid inclusion trails (FIT, planar clusters or clouds of fluid inclusions) and healed microcracks in the blue colored (gamma-irradiated) salt were measured using the universal stage (U-stage). The traces of planar healed microcracks appear as white lines on the thin section surface. The mutual angles between both planar elements and their spatial relationship with the major crystallographic cleavage planes of the corresponding halite grains were analyzed by comparison of the U-stage and EBSD mapping datasets. For this purpose, the Euler angle data describing the crystallographic orientation were converted to dip direction/dip angle data for triplets of <100>, <110> and a quartet of <111> planes. Then, the smallest angle between the pole of the given planar element (FIT or microcrack) and the selected group of crystallographic directions was recorded.

To visualize the sub-micrometric microstructures in particular halite grains at high resolution under SEM microscope, the broad ion beam (BIB) cross sectioning method was used. BIB is an atomic scale erosion process based on Argon source to prepare 2D flat undamaged surfaces (curtaining less than 5 nm deep) up to 2 mm^2, suitable for high resolution SEM imaging of sub-micrometric microstructures (Desbois et al., 2009, 2011a). The grains of interest were sub-sampled from one thin section by dry cutting of small thin section areas (5 × 5 mm^2) using a low speed diamond saw. The BIB cross sections were performed parallel to the plane of the thin section, and coated with gold (15 mA, 50 s) before SEM imaging typically performed at 3 or 7 kV with working distance of 5 mm and aperture of 30 μm.

4. Results

4.1. Description of fabrics and halite grain microstructures

The thin sections of irradiated salt reveal a fabric consisting of alternating 0.5 mm thick bands rich in anhydrite and 5 mm thick bands rich in halite (Fig. 2). The average grain size in halite rich domains is ~300 μm, while in anhydrite rich layers, it is markedly smaller (~50 μm). However, the fabric in both domains is equigranular with axial ratios of the grains ranging between 1.5 and 2.2. Halite grain boundaries are straight or slightly interlobate and often meet at triple point junctions enclosing an angle of 120°. The shape preferred orientation of grains is parallel to the axial planes of isoclinal folds (Fig. 2). The cores of the grains in both domains are marked by pink–violet domains (Fig. 3) that contain straight or chevron shaped arrangements of fluid inclusion trails and less abundant solid inclusions (FIT; see also Figs. 4 and 5). Fluid

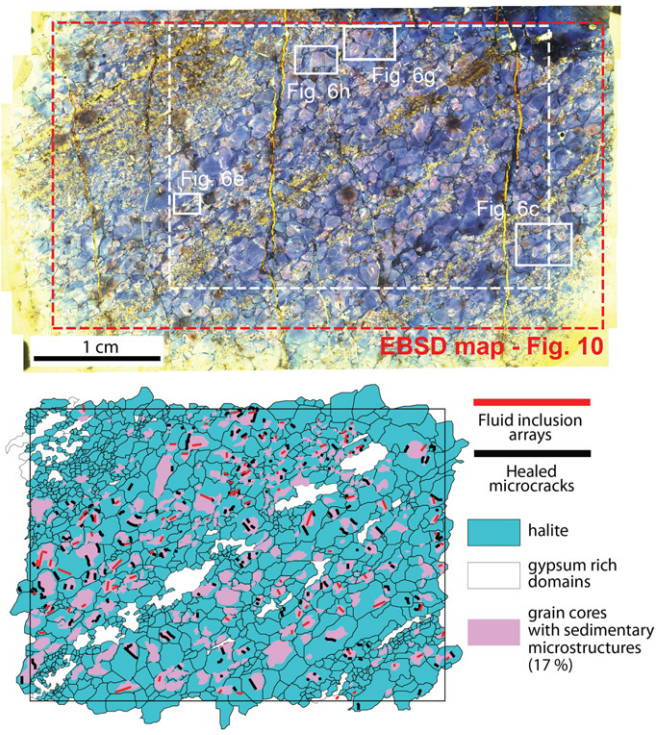

Fig. 2. Micrograph of the entire investigated thin section 1-9b and corresponding digitized microstructure. Extent of the digitized area is indicated by a rectangle with dashed white contour in the micrograph. The extent of EBSD map presented in Fig. 11 is indicated by the red dashed rectangle. Thin section is oriented SW-NE with its long axis corresponding to the horizontal (axis of the borehole). Horizontal right is consistent with the vergence direction of the folds as in Fig. 1c. (For interpretation of the references to colour in this figure legend, the reader is referred to the web version of this article.)

inclusions forming the FITs display pseudo cubic shapes with typical size below 15 μm and form planar cloudy clusters (Fig. 4). Solid inclusions have irregular shapes and are often much larger (20–80 μm) than the fluid inclusions. The pink–violet cores with FITs are surrounded by concentric pale blue mantles and dark blue rims of halite (Fig. 3). The dark blue rims are confined to marginal areas of the grains (Fig. 3) or rarely occur as embayments penetrating the grains from grain boundaries (Fig. 6h). None of the grains revealed sub-grain boundaries.

The FITs are frequently truncated by the following two types of interfaces (Fig. 5): 1) grain boundary between the violet cores of grains containing the FIT and the adjacent grain (Fig. 5a and b), and 2) intra-granular contact between the FIT bearing core and the surrounding pale blue rim (Fig. 5b and c).

The majority of halite grains is marked by white lines that resemble traces of healed microcracks (e.g. Fig. 6) and transect the pale blue mantles, occasionally the cores and only rarely the dark blue rims. Microscopic observations using the U-stage suggest that these white lines represent traces of planar microstructural elements (white planes) that frequently follow the core-pale blue mantle interface and form sub-parallel symmetrical pairs around both tips of the FITs (Fig. 6a, c, e and 7c) and enclose an angle of ~45–55° with the FITs. These white lines clearly attenuate from the core of the grains with FITs toward the grain margins (Fig. 6a, b, e and g). Some of the white lines are relatively thick (up to ~20 μm), irregular and serrated (Fig. 6b, c and g) and can consist of several sub-parallel narrow straight segments in en-echelon arrangements that are locally transected by a long white line (Fig. 6b and c). In some grains, curved white lines encircle the majority (Fig. 6g) or the entire violet core of the grains with

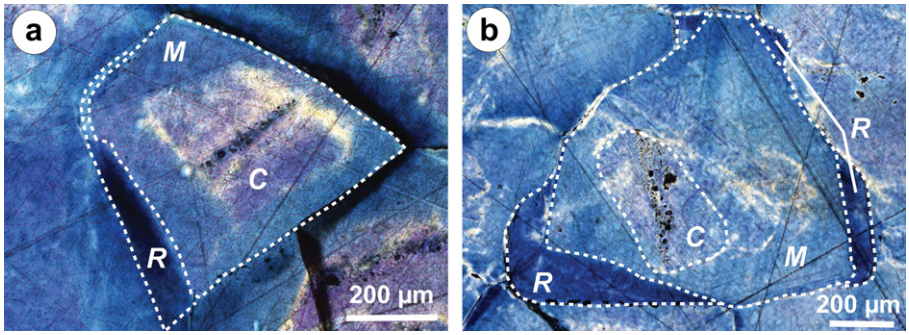

Fig. 3. Concentric core-mantle microstructures (a and b). The pink–violet cores of grains (C) contain straight fluid inclusion trails (FITs). The pale blue mantles (M) and dark blue rims (R) surround the pink–violet cores.

remnant sedimentary fluid inclusion trails (FITs) or reveal hook-shaped terminations (Fig. 6g). A number of white lines clearly emanates from solid inclusions (Fig. 6a), grain boundary ledges (Fig. 6f and 7a–c) or grain boundary triple point junctions (Fig. 6d and 7a, c). In one instance, such a white line is bent and terminates at a grain boundary ledge and the edge of FIT, respectively (Fig. 6f). Some of the white lines cross-cut entire grains (Fig. 7a and b) or delineate closed domains in the margins of the grains (Fig. 7c). In Fig. 7b, a grain is segmented into three domains by two such white lines. While the first of these white lines has curved shape and follows the solid inclusions, the second white line is straight and follows the alignment of FITs. Solid inclusions frequently mark the transgranular white lines (Fig. 7b), white line terminations, or offsets in their straight directional trends (Fig. 6a). Fig. 6e depicts a white line that emanates from a FIT edge in one grain and clearly cross-cuts a grain boundary with adjacent grain and curves and fades out in this neighboring grain.

The white lines contain numerous fluid inclusions of sub-micrometric size distributed in narrow planar clusters (Figs. 6d and 8a). SEM imaging (Fig. 8b) of these fluid inclusions revealed that their shapes are elongated and about few hundreds of nanometer long and few tens of nanometers thick (Fig. 8b1 and b2). Fig. 8b1 reveals efflorescence of fluid inclusions distributed along the white lines leaving behind halite precipitates.

4.2. Quantitative microstructural analysis

Statistical analysis of the digitized microstructure and fabrics (Fig. 2) revealed that the geometrical mean grain size is 257 μm and geometrical mean axial ratio of the grains is 1.61. The violet grain cores with FITs comprise 17% of the thin section area. The preferred orientation of the long axes of the grains at 59° from horizontal is sub-parallel to the layering of the halite- and anhydrite rich bands (Fig. 9a). The traces of white lines in the thin sections reveal a broad maximum centered at an angle 63° from the maximum of long axes of halite grains (Fig. 9b). The alignment directions of FITs produces a slightly irregular rose diagram with three sub-maxima and preferred orientation at 48° from horizontal and 11° from the shape preferred orientation of halite grains (Fig. 9b and c).

The motivation for the EBSD mapping of the thin sections was to characterize (1) the crystallographic fabric of the investigated aggregate, (2) the mutual spatial relationship between the crystallographic lattice of individual halite grains and white intra-granular planar elements and (3) possible misorientation domains within single grains associated with the intra-granular white lines. Inspection of the EBSD maps showed that the pale blue mantles and dark blue margins in individual grains have the same crystallographic orientation as the pink–violet cores with FITs (Figs. 2 and 10). All measured halite grains (Fig. 10) and particularly the population of halite grains containing the white lines lack any preferred crystallographic orientation (Fig. 12). Detailed inspection of the EBSD map in thin section 1-18b also revealed that the grain with three parallel FITs, transected by curvy and straight white lines depicted in Fig. 7b, consists of three domains that are slightly (<10°) mutually misoriented as shown on associated misorientation profiles (domains a–c in grain 2 along A–A′ profile in Fig. 11). Another profile in the EBSD map of thin section 1-9b (B–B′ in Fig. 11) that corresponds to the inset in Fig. 6e, revealed a 15° misorientation between two grains or two domains of a single grain (domains 1 and 2). This lattice discontinuity corresponds to the location of one white line that is a tangent to the FIT and transects the grain at about 45° to the FIT (Fig. 11).

Comparison of the mutual spatial relationship between the white intra-granular planar elements (white planes), FITs and

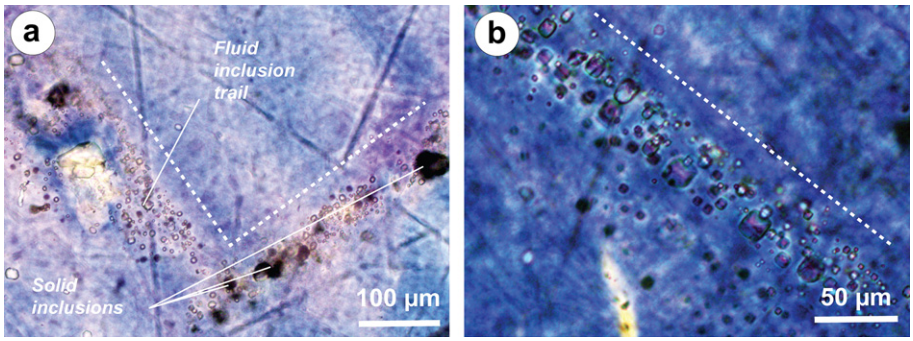

Fig. 4. Details of sedimentary fluid inclusion trails (FITs) in pink–violet cores of the grains. (a) Chevron shaped fluid inclusion trail is indicated by white dashed line. The solid fluid inclusions appear black. (b) The trend of straight shaped FITs is indicated by white dashed line.

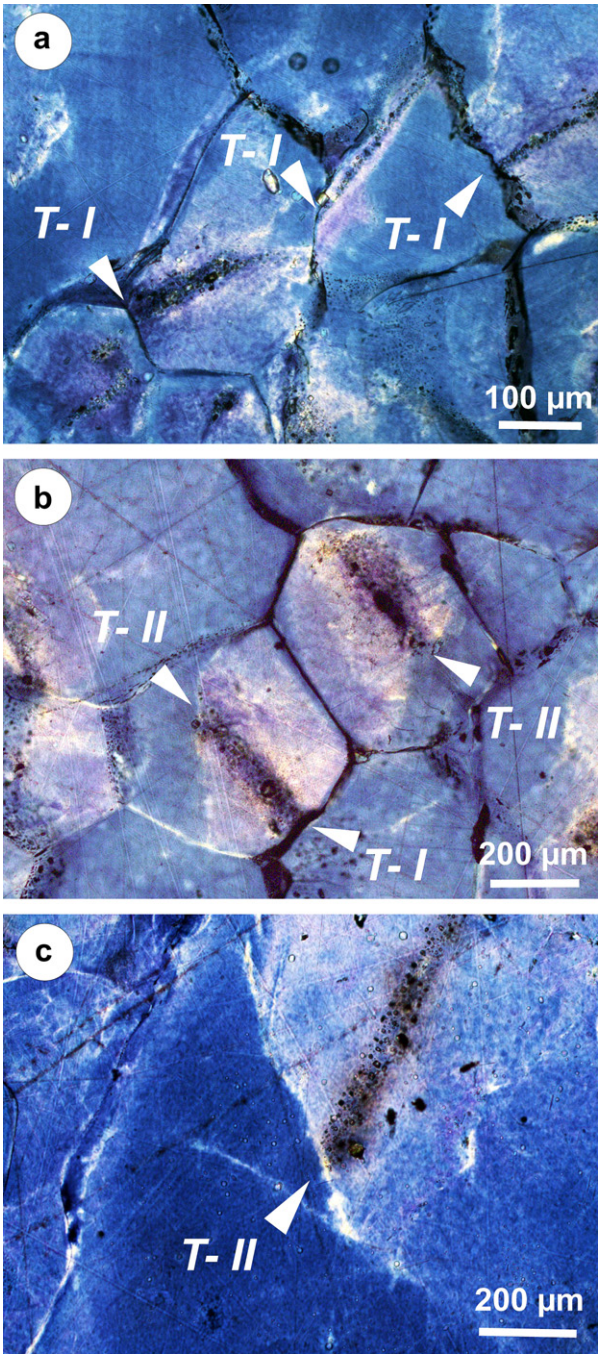

Fig. 5. Truncation of sedimentary fluid inclusion trails (a–c). Two types of truncation patterns are identified in the micrographs: the first (T-I) is defined by inter-granular contact of the pink–violet core bearing the fluid inclusion trail with adjacent grain, while the second (T-II) is characterized by intra-granular contact between the FIT and pale blue mantle. Note a white line following the pink–violet core and pale blue mantle interface in (b) and (c).

crystallographic directions of associated halite grains revealed that, (1) FITs follow the (100) planes of halite crystals (Fig. 13a), (2) the mutual angle between the white planes and the FIT in the corresponding grain has a Gaussian distribution centered at approximately 52° (Fig. 13b) and, (3) alignment of white planes do not show any affinity with respect to the major crystallographic cleavage planes of halite (Fig. 13c). The statistics of the mutual angle between the white planes and corresponding halite cleavage planes (Fig. 13c) revealed log-normal distribution and maxima of about 45° with respect to (100), 30° with (110) and 15° with the (111) planes of the halite grains. These angular relationships can be simplified into a single crystallographic plane in the halite crystal lattice defined by the Miller indexes [13,10,8].

5. Discussion

5.1. Interpretation of microstructures

Similarly to Schléder et al. (2008), straight and chevron shaped FITs in pink–violet cores (C) are interpreted as primary fluid inclusions from relicts of sedimentary primary grains crystallized during the deposition of the rock salt sequence. Different color intensities of pale blue mantles and dark blue rims surrounding the primary fluid inclusion rich violet cores reflect two different events of halite precipitation in agreement with the physical principle of gamma-irradiation method used to decorate the samples (Urai et al., 1987; Celma and Donker, 1996; Schléder and Urai, 2007; Schoenherr et al., 2010; Desbois et al., 2010). The zonality of grains defined by the distribution of the cores, pale blue mantles and dark blue rims (Fig. 3) indicates that the pale blue mantles postdate the violet cores and predate the dark blue rims. The core and pale blue mantle interfaces (Figs. 3, 5 and 6) reflect the early corrosion by indenting grains or possibly zones of brittle failure of the old grains that developed during compaction of the Werra salt layer prior to precipitation of pale blue mantles. Interfaces between violet cores and adjacent grains (Fig. 5a and b) are interpreted as partial dissolution surfaces of indented grains.

All the white lines (white planes) in the blue – gamma-irradiated Neuhof salt aggregate are interpreted as healed microcracks or microfractures in general due to the following reasons: 1) the morphology and locations of these microstructural elements is similar to microcracks that develop around lattice imperfections and grain boundaries due to stress accumulations (Kranz, 1983), 2) these planar elements contain arrays of fluid inclusions distributed in planar clusters (Fig. 8), which is supported by efflorescence patterns on the cross sections prepared by the BIB method (Fig. 8b1 and 3) absence of blue coloration along these elements reflects accumulation of H-centers (Cl_2 molecules) characteristic for lattice discontinuities like sub-grain boundaries (Urai et al., 1987; Celma and Donker, 1996; Schléder and Urai, 2007). Correlation of the microstructures with corresponding EBSD maps also shows that the majority of the "white lines" represent traces of healed microcracks, because these did not produce any lattice misorientations. In contrast, transgranular discontinuities in grains (Fig. 11), along which slip occurred, correspond to microfractures that became new grain boundaries.

The fluids distributed along the microcracks likely originate either from grain boundary brine or fluids stored in the fluid inclusion trails (FITs) that were mobilized by pressure gradients during opening of the cracks and were isolated by later healing process (Hickman and Evans, 1991; Lehner, 1995; Ghoussoub and Leroy, 2001; Schenk and Urai, 2004; Desbois et al., 2011b). Termination and truncation of numerous intra-granular microcracks at the interfaces of pale blue mantles and dark blue rims (Fig. 6c) suggests that the microcracking event in pale blue mantles was followed by partial corrosion of these mantles before precipitation of the dark blue rims.

5.2. Solution-precipitation creep and grain boundary sliding (SP–GBS)

Solution-precipitation (SP) creep was already found as the dominant deformation mechanism in the Neuhof Werra salt (Schléder et al., 2008). This contribution confirms the coupled

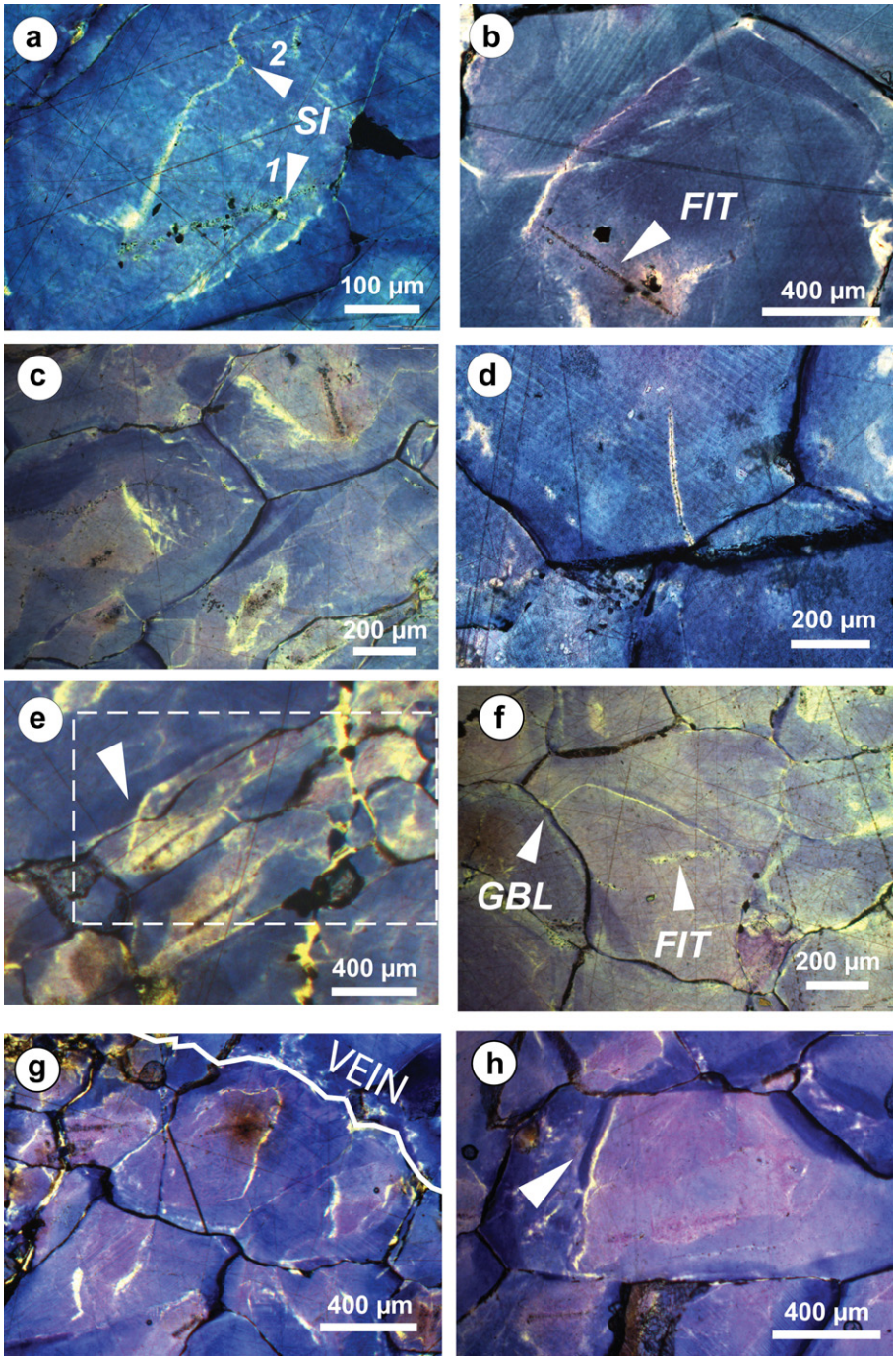

Fig. 6. Micrographs illustrating the morphological diversity of the microcracks (white lines in micrographs) identified in the folded perennial Werra salt from the underground Neuhof-Ellers salt mine. All micrographs are oriented SW-NE and formed during top to the right sense of simple shear in the halite aggregate. White straight microcracks are frequently developed at an angle of ~45° to the FITs (a, e, g). (a) Grain, where a large solid inclusion (SI) marks a tip of a microcrack (arrow 1), while second microcrack on the opposite side of FIT is offset from a straight course at another solid inclusion (arrow 2), (b) Microcrack perpendicular to adjacent fluid inclusion trail (FIT) displaying an en-echelon arrangements of distal segments. (c) Several grains showing intra-granular damage developed along the purple and pale blue salt interface in individual grains. (d) Microcrack at a grain boundary triple junction. (e) Grain with microcrack emanating from FIT at ~45° and cross-cutting adjacent grain boundary is indicated by arrow. Dashed rectangle indicates the EBSD map inset in Fig. 11. (f) Curved microcrack that spans from a grain boundary ledge (GBL) to a far end tip of fluid inclusion trail (FIT). (g) Detail of several grains showing intra-granular microcrack with hook-shape endings and microcrack that encircles half-way the core of the largest grain. The wall of an adjacent vein that penetrated the folded sequence (Schléder et al., 2008) is indicated by a thick white line. (h) Dark blue salt embayment (arrow) parallel to adjacent microcrack, both localized at the violet core-pale blue mantle interface. (For interpretation of the references to colour in this figure legend, the reader is referred to the web version of this article.)

activity of both pressure solution, evident from corrosion of violet core-pale blue mantle and pale blue mantle-dark blue rim interfaces and FIT truncations, and precipitation of pale blue mantles and dark blue rims in the polycrystalline aggregate. The measured random crystallographic preferred orientation of the halite grains (Figs. 10 and 12) fully corroborates the dominant SP deformation mechanism (Passchier and Trouw, 2005; Schléder and Urai, 2007; Desbois et al., 2010).

The extreme fluidity of the perennial Werra salt sequence in contrast to the adjacent rock salt sequences was earlier attributed

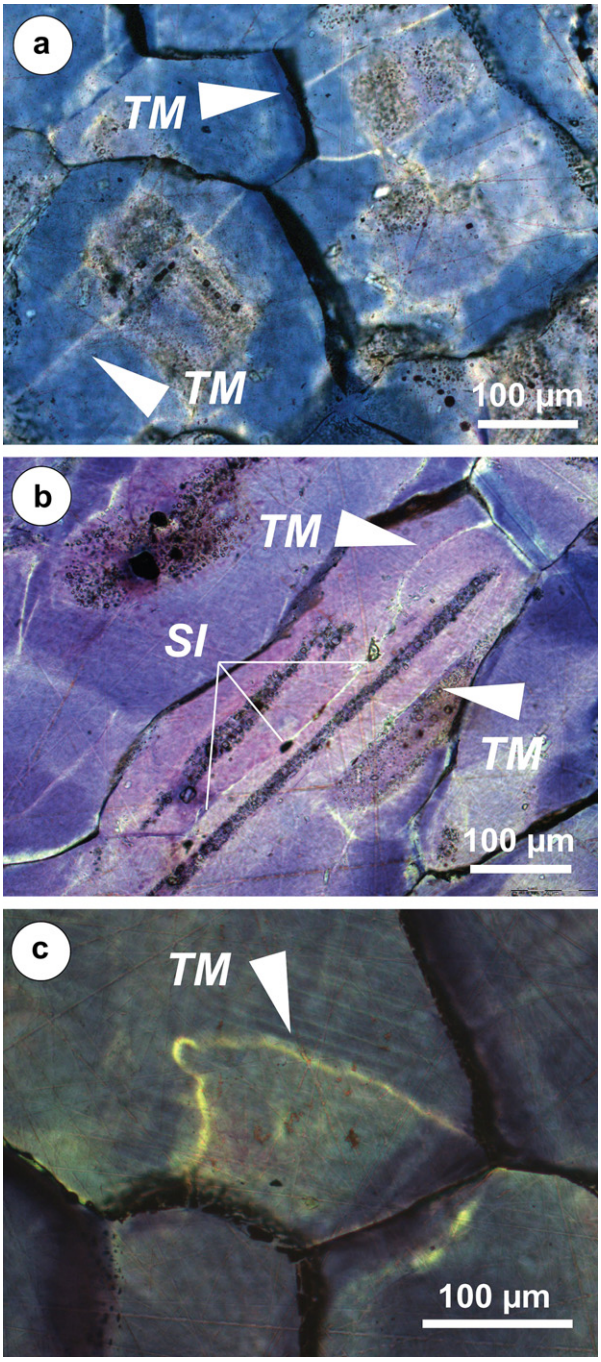

Fig. 7. Transgranular microcracks (white lines in micrographs). (a) Transgranular microcracks through violet core and pale blue mantle domains. (b) Two transgranular microcracks (TM) cross-cutting the violet core and pale blue mantle domain. Note that the curved microcrack follows the solid inclusions (SI). (c) Transgranular microcrack (TM) connecting a grain boundary triple point junction and a grain boundary ledge, respectively that encompasses relatively small domain of the grain. (For interpretation of the references to colour in this figure legend, the reader is referred to the web version of this article.)

to its small grain size of 500 μm and the SP–GBS creep at strain rates of up to $5 \times 10^{-10}\,s^{-1}$, for temperature $T = 80\,^{\circ}C$ (Schléder et al., 2008). Our refined grain-size measurement of 257 μm suggests even higher strain rates of $3.7 \times 10^{-9}\,s^{-1}$ (Spiers et al., 1990). These calculated strain rates are one order of magnitude higher than those suggested for salt glaciers (Schléder and Urai, 2007) and one order of magnitude slower than the slowest experiments performed on wet halite (Spiers et al., 1990). Poirier (1985) explains that "the diffusion of matter along grain boundaries during diffusion creep creates the driving force for grain boundary sliding (GBS) and vice versa. Both, diffusion creep and GBS are therefore strongly coupled and mutually accommodated; one cannot exist without the other". We suggest, that the same mutual dependence is also valid for SP and GBS mechanisms in the Werra salt, because SP creep involves diffusion around grain boundaries and flow laws for diffusion creep and SP creep are similar (Blenkinsop, 2000). Coupled activity of SP creep and GBS is typical with low degree of CPO and abundant substructure-free grains (Schléder and Urai, 2007; Desbois et al., 2010).

The comparison of the Werra rock salt in contrast to extrusive rock salts is particularly interesting, because both reveal deformation dominantly by SP–GBS coupled creep. However, the underground Werra salt representing the source layer (or mother salt) was constrained by relatively higher confining pressures and possibly mobilized by higher differential stresses than typical for extrusive salts (Schléder and Urai, 2007; Desbois et al., 2010).

5.3. Microcracking mechanisms in the Werra rock salt

The discussion of the physical mechanism controlling the development of microcracks and microfractures, first requires interpretation of the kinematic framework of the Werra rock salt deformation. The origin of microcracks will be then evaluated on the basis of their morphological characteristics, their position and orientation and timing of their formation during the Werra rock salt deformation. The degree of differential stress during the Werra salt deformation cannot be constrained by paleopiezometry (e.g. Carter et al., 1993), due to absence of sub-grains. However, experiments of Urai et al. (1986) revealed that artificial salts of similar grain size (200 μm) deformed at 70 °C and strain rates that are one order of magnitude higher than estimated in this study, can withstand flow stresses up to 1 MPa in PS-GBS creep regime.

The NE vergence of isoclinal folds (Fig. 1b) in the Werra salt suggests that the flow of this rock salt was non-coaxial, with top to the NE simple shear and the folds are a product of passive folding, where anhydrite layers acted as passive markers (Price and Cosgrove, 1990). We assume that the maximum compressive stress was directed perpendicular to the layering and grain shape fabric (Fig. 9b) in the Werra salt, because grains are elongated in direction perpendicular to maximum compressive stress during SP creep (Passchier and Trouw, 2005). This direction also complies with the average direction of a broad maximum of the traces of microcracks in the 1-9b thin section (Fig. 9b). The origin of microcracks and microfractures in rock salt is generally attributed to dilatancy and fluid overpressure induced dilatancy (Renner et al., 2000; Peach et al., 2001; Schoenherr et al., 2007; Urai and Spiers, 2007). Besides the dilatancy, we also consider the mechanism of Griffith (1921) crack propagation due to stress accumulations around lattice imperfections in the grains and the cavitation mechanism resulting in accumulation of creep damage and "ductile tearing" of polycrystalline aggregates (Mitra, 1978; Čadek, 1988; Závada et al., 2007; Rybacki et al., 2010).

There are four types of microcracks recognized in this study: 1) intra-granular microcracks that emanate from both tips of FITs, which attenuate to the grain margins (Fig. 6a and b) and locally cross-cut boundaries with neighboring grains (Fig. 6e and 11); 2) relatively thick intra-granular microcracks with serrated boundaries and splaying edges (Fig. 6c), 3) microcracks that encircle the majority of the violet cores or display hook-shaped terminations, and 4) microcracks emanating from grain boundary triple point junctions (Fig. 6d) or grain boundary ledges (Fig. 6f) that can be transgranular (Fig. 7). Only the second type of

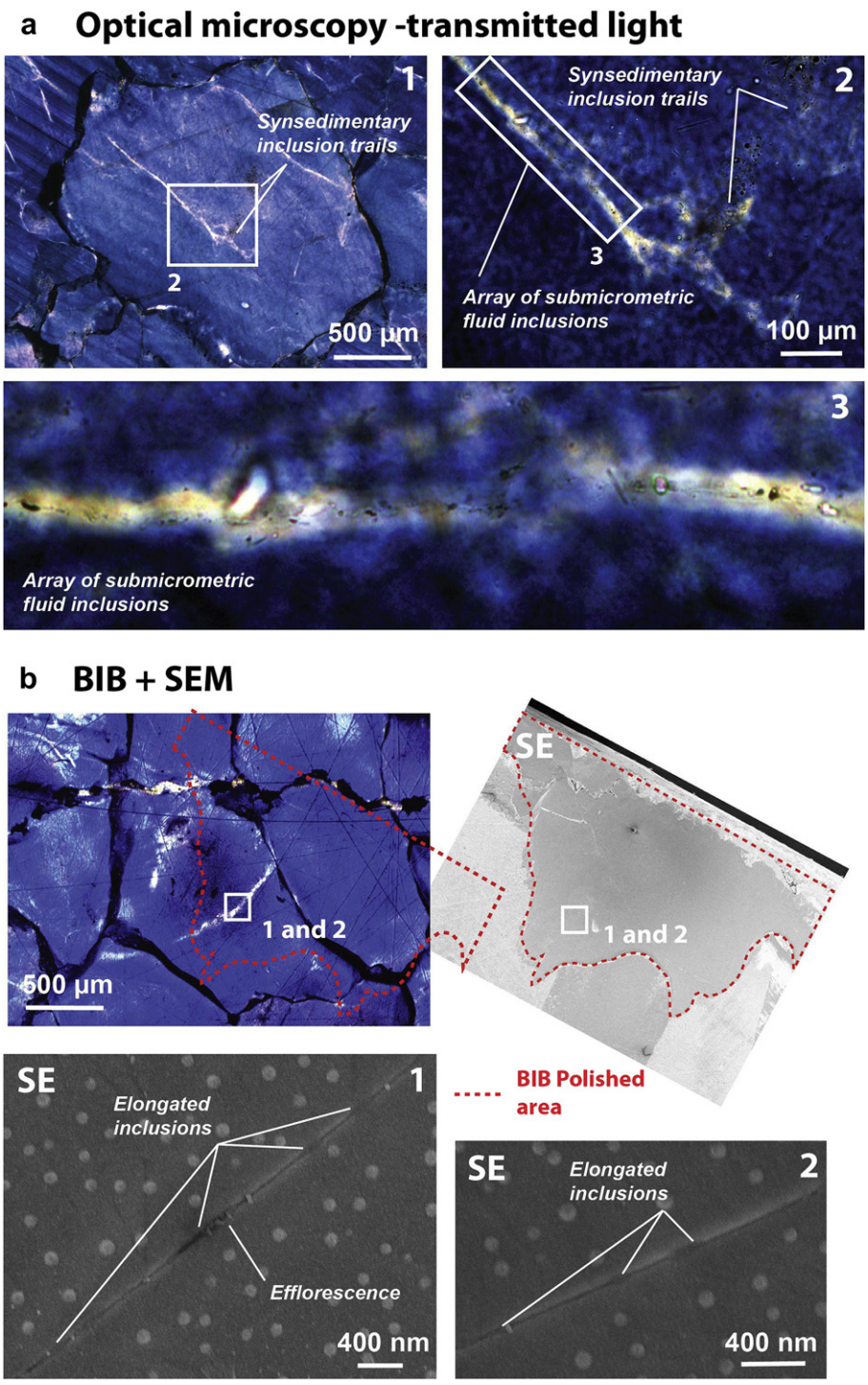

Fig. 8. High magnification details of microcracks (white lines); (a) under optical microscope in transmitted light, microcracks show a planar array of sub-micrometric fluid inclusions, (b) SEM micrographs reveal microcrack containing elongated inclusions about 400 nm long with efflorescence pattern in their direct vicinity.

microcracks (thick with serrated boundaries) developed sometimes between the precipitation events producing the pale blue mantles and dark blue rims around the violet cores. The first and fourth type of microcracks likely originated during the last stages of Werra rock salt deformation, because some of them are closely spatially associated with the grain boundaries or even cross-cut these boundaries (Fig. 6d–f). The timing of development of the third type of microcracks cannot be constrained.

Regarding the first type of microcracks, the fact that these attenuate from the edges of FITs toward grain boundaries and that some of them cross-cut boundaries with adjacent grains (Figs. 6e and 11) suggest that these propagated from the tips of FIT outwards and originated as Griffith cracks initiated from solid or fluid inclusions at the edges of the FITs due to flow stress concentrations. This scenario is possible for Werra rock salt, because Griffith (1921) showed that even when the applied stresses are compressive, the

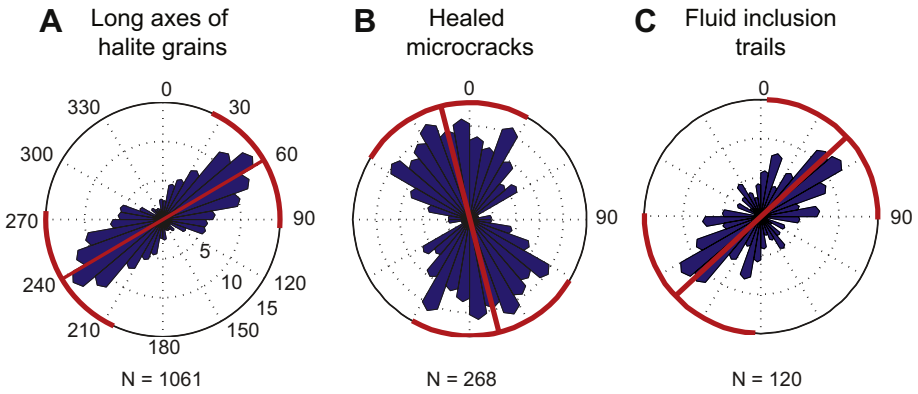

Fig. 9. Rose diagrams revealing the preferred orientation of (a) long axes of halite grains, (b) traces of microcracks (white lines) and (c) fluid inclusion trails (FITs), traced from the 1-9b thin section (Fig. 2). Number of digitized linear elements is indicated below each rose diagram. The 0 and 90° in the rose diagrams correspond to the vertical and horizontal in the direction of folds vergence, respectively, as in Fig. 1c and 2.

'tip' stresses around elliptical flaws would be tensile. The entire planar clusters of solid and fluid inclusions forming the FITs are interpreted as inhomogeneities similar to Griffith's elliptical voids, although the microcracks finally propagate from single solid or fluid inclusions at the tips of the fluid inclusion array (e.g. Fig. 6a). The angle of ~52° between the FITs and the microcracks likely reflects the relatively high angle of the FITs with respect to the maximum compressive stress direction during flow of the Werra rock salt layer in agreement with experimental results on cracking of isotropic materials with pre-manufactured slots (Chan et al., 1996; Kozak et al., 1981). The second "white line" encompassing the right side of FIT in the grain in Fig. 6e (also Fig. 11) is again aligned at about 40–50° to the FIT and corresponds to intra-granular lattice discontinuity dividing the pale blue mantles and dark blue rims (Fig. 11). This discontinuity with 15° misorientation angle can be regarded as an incipient new grain boundary and can be interpreted as a transgranular crack, along which slip between the lattice domains occurred.

The second type of microcracks (thick microcracks with serrated boundaries and splaying edges) can be interpreted as a dense cluster of en-echelon, Griffith-type tensional microgashes that developed along the violet core-pale blue mantle interface and coalesced into a single thick damaged zone, which subsequently healed. The violet core-pale blue mantle interface probably represents a low cohesion surface, along which microcracks preferentially develop and propagate, because the sedimentary violet cores are likely more abundant in pores and impurities than the pale blue mantles. The serrated and splaying edges of microfractures in grains depicted in Fig. 6c likely reflect the interaction of conjugate sets of Griffith-type microcrack arrays. Alternative explanations for these crack patterns are dilatancy or fluid induced dilatancy (Peach and Spiers, 1996; Popp et al., 2001; Schoenherr et al., 2007) causing opening of cracks from grain boundaries into the grains during the early stages of Werra rock salt deformation or the crack-seal mechanism (Ramsay, 1980) of old grain boundaries between grains in dilating aggregate. Regarding the latter mechanism, the microcrack pattern should be more regular and its filling should display zonality (Ramsay, 1980).

The third type of microcracks – encircling the violet cores could reflect either that: (1) the propagation of microcracks was much easier along the violet core-pale blue mantle interface than through the pale blue salt, and/or (2) the growth of cracks occurred stepwise during the SP–GBS creep, each time at different orientation of the host grain with respect to the maximum compressive stress direction. The hook-shaped terminations of microcracks (Fig. 6g) in three grains adjacent to the halite vein wall could also reflect growth of "daughter" cracks (Kranz, 1983) from tips of preexisting cracks in response e.g. to elastic stresses developed during opening of an adjacent vein (Fig. 1c), which cross-cuts the folded Neuhof salt at high angle to the halite fabric (Schléder et al., 2008).

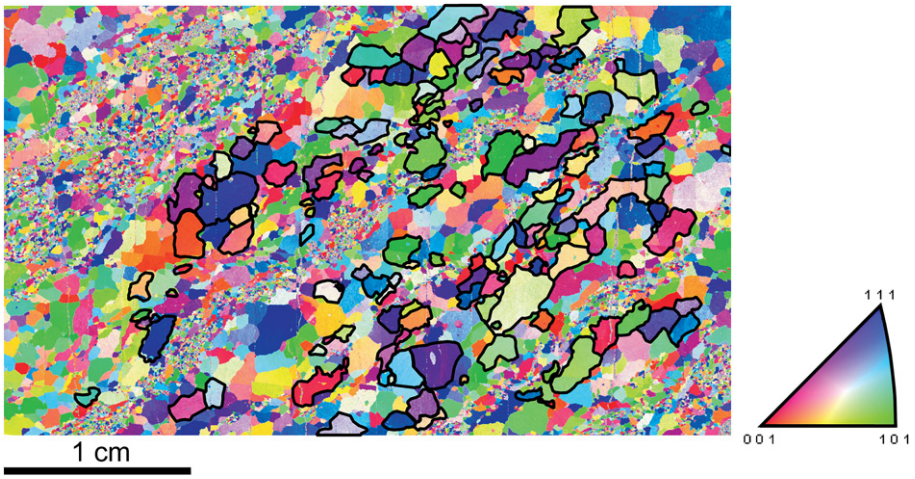

Fig. 10. EBSD map of thin section 1-9b color coded according to the inverse pole figure on the right side of the image. Fractured grains selected for U-stage measurements of intragranular fractures (146 grains) are indicated by a thick dark contour. The extent of the EBSD map corresponds to the dashed rectangle in micrograph of Fig. 2.

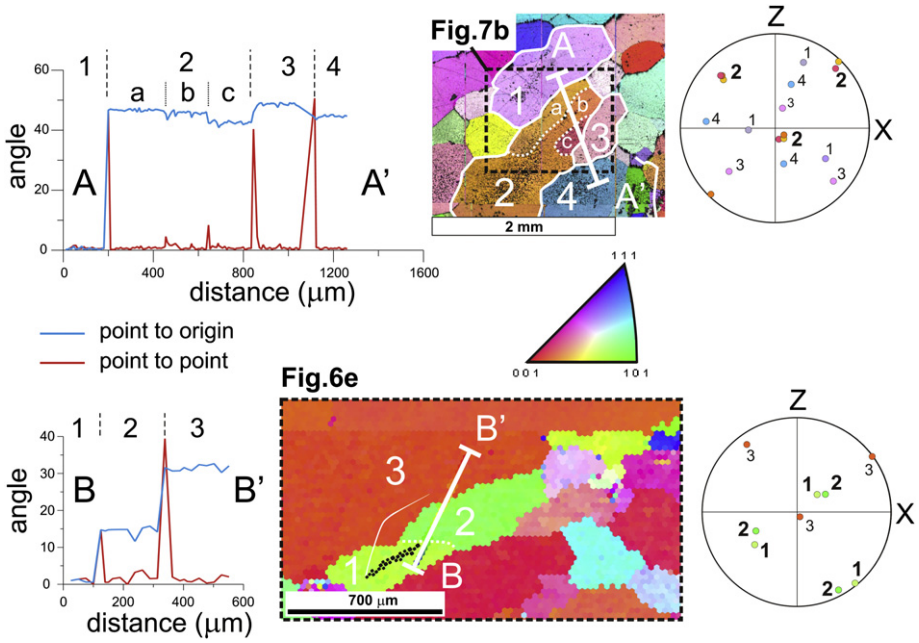

Fig. 11. EBSD map insets corresponding to micrographs in Figs. 6e and 7b with indicated lattice misorientation profiles and stereographic projections of 001 crystallographic directions for corresponding halite grains and their domains. The low angular misorientation steps of lattice domains across profile A–A′ correspond to location of the two longitudinal transgranular microcracks (Fig. 7b) transecting the profile. Note that the individual grains that are transected by profile A–A′ are designated by numbers 1–4. Profile B–B′ reveals a 15° misorientation angle across a grain boundary between grains 1 and 2. This grain boundary likely corresponds to a former intra-granular lattice discontinuity represented by a transgranular microcrack (indicated by a white dashed line), along which the grain domains 1 and 2 later rotated. Note that the curved white line (microcrack) transecting grain boundary with grain 3 and a fluid inclusion trail visible in Fig. 6e were drawn on the EBSD inset. 'Point to origin' marks the misorientation angle value of halite lattices along the profile with respect to that in the origin of the profile. The 'point to point' curve marks the misorientation angle between adjacent points along the profiles. Note that negative misorientation angles along given rotational axes are subtracted from the cumulative value of the 'point to origin' profile, therefore the local misorientation angles (point to point) do not always add up to the cumulative value (point to origin). The misorientation angle values between and within the designated grains and corresponding crystallographic orientation of rotational axes are as follows: Misorientation profile A–A′ (Fig. 7b): 1–2: 46.8° < $\overline{23}$ $\overline{9}$ $\overline{11}$ >; 2(a–b) 4.3° < 18 $\overline{19}$ $\overline{9}$ >; 2 (b–c): 8° < 1 16 1 >; 2–3: 37.7° < 11 $\overline{14}$ $\overline{1}$ >; 3–4: 50.2° < 15 $\overline{7}$ $\overline{7}$ >. Misorientation profile B–B′ (Fig. 6e): 1–2: 13.8° < 12 $\overline{7}$ 15 >; 2–3: 41.4° < $\overline{17}$ $\overline{3}$ $\overline{5}$ >.

The fourth type of microcracks can be attributed to stress concentrations that develop at grain boundary irregularities (triple point boundary junctions or grain boundary ledges) during grain boundary sliding (Kranz, 1983; Kassner and Hayes, 2003; Závada et al., 2007). Comparison of micrographs (Fig. 7b) and corresponding EBSD map insets (Fig. 11) suggests that new grains can form by rotation of lattice domains along such lattice discontinuities.

Another mechanism that was considered for the development of intra-granular microcracks in the Werra salt is the process of cavitation (Mitra, 1978; Čadek, 1988; Kassner and Hayes, 2003). This mechanism produces damage of aggregates similar to that produced by dilatancy, but occurs in the realm of ductile flow and creep dominated by GBS, while dilatancy is generally associated with dynamic recrystallization and semibrittle failure (Peach et al., 2001; Urai and Spiers, 2007; Niemeijer et al., 2010). Since intra-granular cavitation damage is generally associated with crystallographically oriented dislocation pile-ups at lattice discontinuities represented by solid or fluid inclusions or grain boundaries (Kassner and Hayes, 2003; Závada et al., 2007), it is expected that these should follow some specific crystallographic planes, perpendicular to one of the active slip systems (Závada et al., 2007). The cavitation process can be excluded in case of the Werra rock salt microstructure, because (1) the microcracks do not show any logical spatial relationship with the typical halite slip systems {1 1 0}< 1 $\overline{1}$ 0 >, {1 0 0}<0 1 1> or {1 1 1}< 1 $\overline{1}$ 0 > (Wenk et al., 2009) and, (2) such damage should be regularly distributed along the entire fluid inclusion trails, not only around the marginal fluid inclusions in the array.

5.4. Development of halite grain microstructures during the halokinesis of the Werra rock salt layer

The interpreted development of halite grain microstructures during halokinesis of the investigated Werra rock salt layer is summarized in a schematic diagram in Fig. 14. The pink–violet cores of the grains in the investigated Werra rock salt with planar or chevron shaped FITs along the [100] cleavage planes of halite represent the relicts of primary grains that deposited in the perennial lake (Fig. 14a). It is possible that already during the diagenesis and compaction of this rock salt, numerous grains broke up due to stress concentrations at contacts between the grains of the porous rock salt aggregates.

During the incipient halokinesis and the first stage of SP–GBS coupled creep (Fig. 14b), the primary grains were corroded by solution along grain boundaries with adjacent grains and new salt precipitated around the cores from the inter-granular brine solution producing the pale blue mantles. Then, intra-granular microcracks developed preferentially at the tips of FITs and propagated at an angle of 52° from the FITs. Evidence for new grain boundaries that develop from transgranular cracks at FIT tips (Figs. 6e and 11) and the fact that the intra-granular microcracks (Fig. 14b1) grew along the violet core-pale blue mantle interfaces in several grains (e.g. Fig. 5b and c) may further suggest that these interfaces represent zones, along which intra-granular failure occurred more than once during the entire halokinesis event of the Werra rock salt. Multiple failures of intra-granular interfaces are further supported by microstructural evidence from a grain in Fig. 6h, where

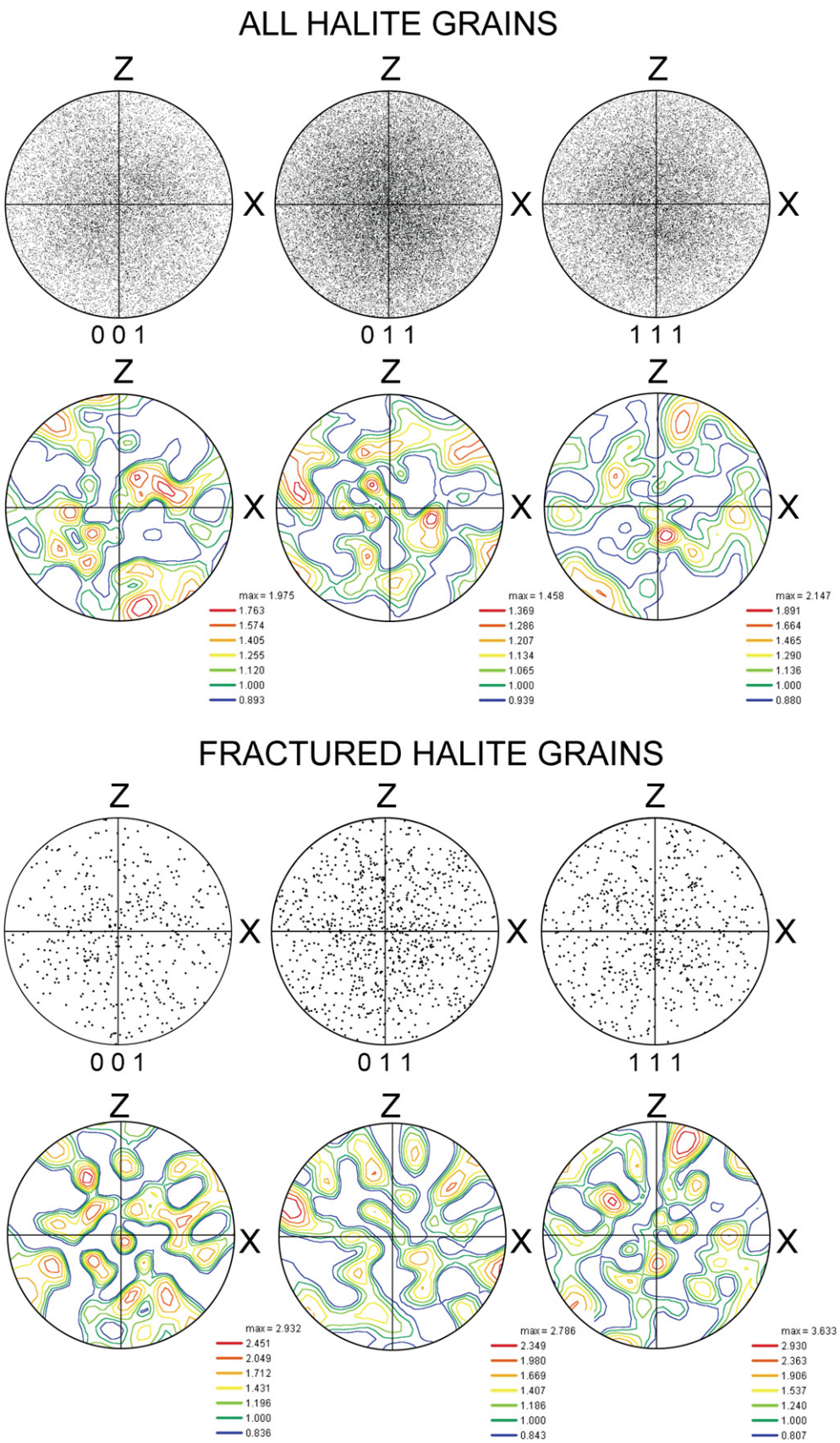

Fig. 12. Lower hemisphere, equal area stereographic projections of the major crystallographic directions for 6800 halite grains measured in the EBSD map (Fig. 10) and 146 fractured grains (indicated by thick black contour in Fig. 10). All projections are characterized by random distribution of the major crystallographic directions of the halite grains. The *Z* and *X* directions correspond to the vertical and horizontal edge, respectively, of the measured thin section (Fig. 2).

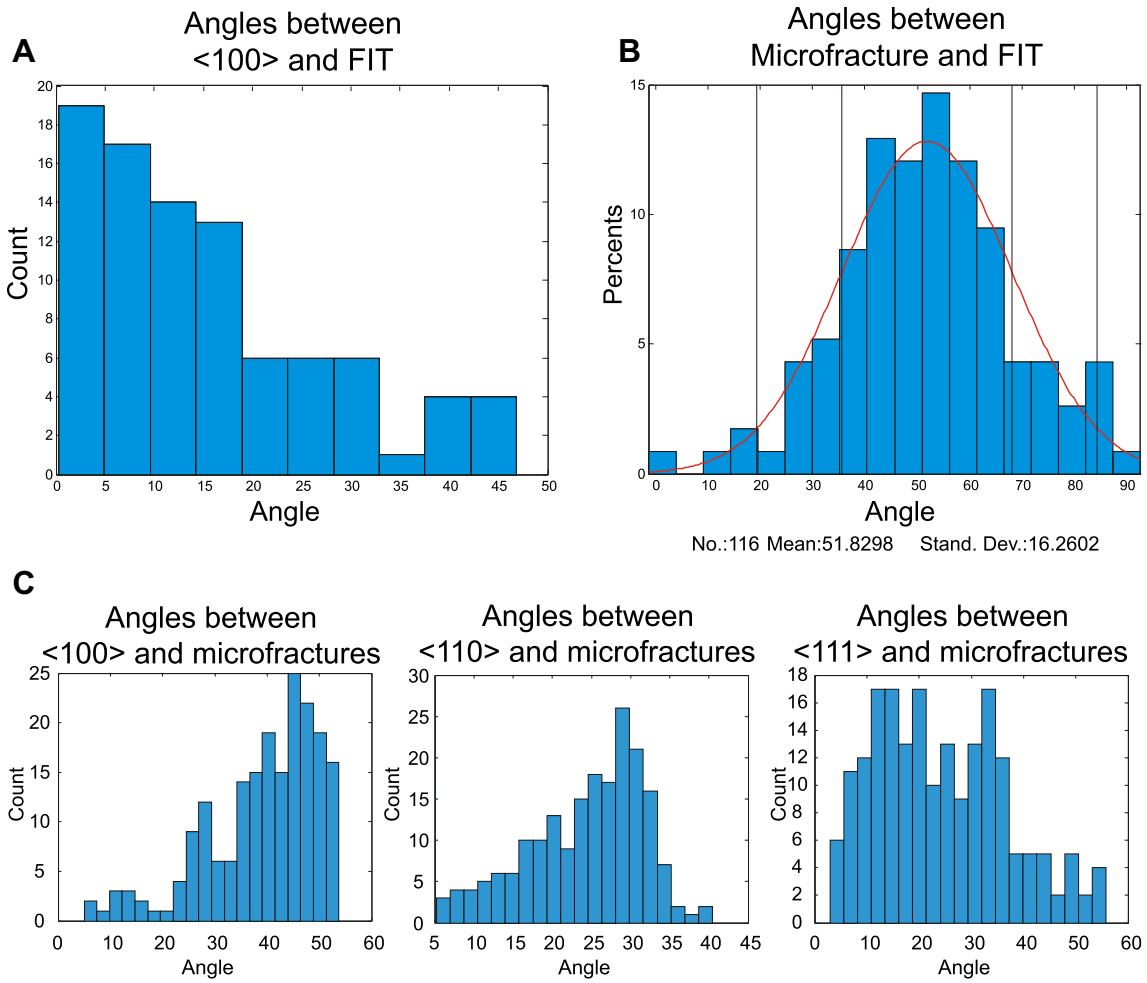

Fig. 13. Histograms showing angular relationships between planar microstructural elements (FITs and microcracks) measured in individual grains and selected crystallographic planes of halite (<100>, <110>, <111>) and mutual angles between the FITs and microcracks (b). Maximum distribution of angles close to 0° in the first histogram (a) suggests that the fluid inclusion trails (FITs) follow preferentially the <100> planes of halite crystals. Microfracture vs. FIT angles reveal a regular Gaussian distribution with maximum of 52° (b). Comparison of microcracks vs. selected cleavage planes of halite crystals reveals log-normal distributions (c). Note that the microcracks do not reveal any affinity to the selected cleavage planes. The smallest angle between the respective microstructural element and one plane in the triplet of equivalent crystallographic planes was plotted. Total 195 fractures and 90 fluid inclusion trails within 146 grains were measured and compared with crystallography of corresponding grains.

a microcrack follows an embayment of dark blue salt, possibly representing precipitated fluid phase in a cavity developed by a break-up of the grain. Both, the crack and the dark blue salt embayment follow the violet core-pale blue mantle interface.

By continued folding and SP–GBS creep (Fig. 14c), transgranular microcracks dissect some of the grains across the pale blue mantles (Fig. 14c1) or across both violet cores and pale blue mantles (Fig. 14c2). At this point, the grain boundary network incorporates new brine from the intra-granular fluid inclusions cross-cut by transgranular microcracks (Fig. 14c2) or excavated by non-conservative GBM (Fig. 14c3). New ingress of brine and decreased grain size by transgranular microcracking enhanced a second stage of SP–GBS creep resulting in precipitation of dark blue rims on corroded and microcrack bearing pale blue mantles.

5.5. *Transient failure of the perennial rock salt and enhancement of SP–GBS mechanism*

The interpretation of evolution of the Werra rock salt aggregate implies an interesting mutual interplay of the mechanical (microcracking) and chemical (solution and precipitation) processes that govern its rheological behavior. Microcracking of the halite aggregate promotes the SP creep by the following processes; (1) creation of new grain boundaries (Fig. 7 and 11), where microcracks transect the grains, causing grain-size reduction and, (2) the incorporation of sedimentary trapped fluids into the grain boundary network when FITs are cross-cut by transgranular microcracks (Fig. 7). More over, continuous SP creep was also facilitated by input of brine into grain boundaries, where the FIT bearing cores of grains were excavated by the non-conservative GBM (Fig. 5). The mutual interaction between microcracking and SP processes likely produced a step-wise strength decrease and non-steady state flow of the Werra salt, which is governed by the composite nature of individual grains. In other words, grain-size decrease (Carter et al., 1993; Spiers et al., 1990) and redistribution and ingress of fluids stored along FITs (Jackson, 1985; Urai et al., 1987; Urai and Spiers, 2007) induced by microcracking, facilitated continuous deformation of the aggregate at low differential stress. The absence of intra-granular microcracks in the dark blue salt domains in marginal parts of the grains suggests that the SP–GBS process in the halite aggregate was not terminated at the time of their formation. Therefore, the origin of these microcracks does not mark the final creep failure state, but rather a transient failure of the halite aggregate. The concept of step-wise decrease in strength

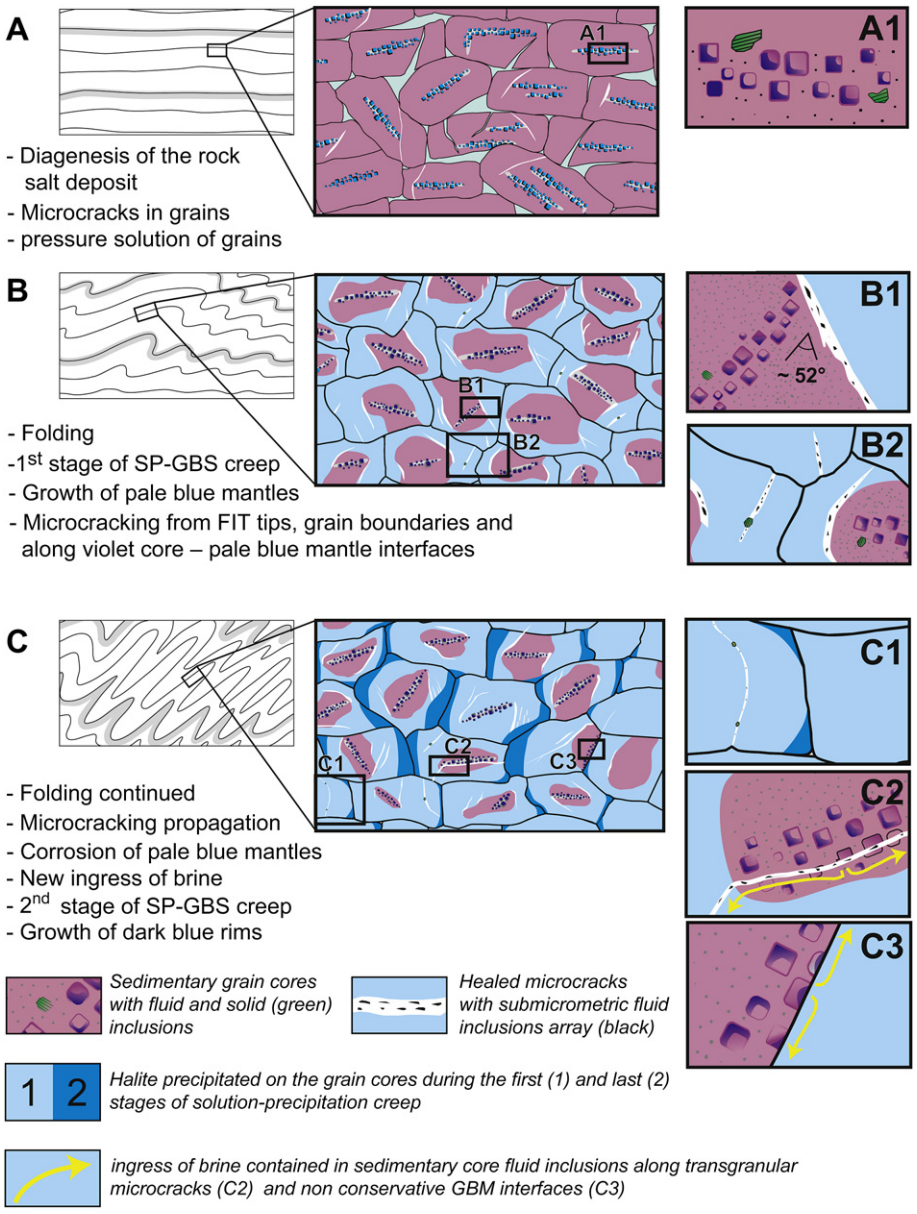

Fig. 14. Schematic diagrams depicting the evolution of the microstructure during the halokinesis of the Werra rock salt layer. (a) Deposition in the perennial-lake environment produces accumulations of rectangular halite flakes with enclosed fluid inclusion trails (FITs) along the [100] cleavage planes of halite. Compaction and diagenesis of the early deposit likely accumulates stresses at grain contacts that produce transgranular cracks. (b) Incipient flow of salt is accommodated by solution-precipitation (SP) creep coupled with grain boundary sliding (GBS). Microcracks (in white) develop preferentially at the tips of FITs and propagate at an angle of 52° with respect to FIT and/or along the interfaces of FIT bearing cores of grains and newly precipitated salt (insets B1 and B2). Other microcracks originate at grain boundary triple point junctions or grain boundary ledges (inset B2). (c) Continuation of SP–GBS creep produces partial solution of the damaged grains and precipitation of new salt indicated by dark blue colors. The continuation of SP–GBS is facilitated by input of brine into the system from the FITs, where the microcracks cross-cut the grain cores along the FITs (inset C2) or where the FITs were excavated by non-conservative grain boundary migration (inset C3). Microcracking decreases the average grain size of the aggregate (inset C1), further promoting the SP–GBS creep at lower flow stresses. See text for more details.

inferred from microstructural observations in the Werra perennial salt resembles the complex interplay between mechanical weakening (brittle fragmentation, milling of grains) and chemical strengthening (healing of inter- and intra-granular voids by precipitation of halite during SP) of experimental halite fault gauges described by Niemeijer et al. (2010).

5.6. Implications for rheology of rocks governed by GBS

Our results suggest that microcracking is a significant process that accompanies the SP–GBS and can therefore contribute to the understanding of the general principles controlling rheology of rocks deforming by GBS – assisted mechanisms in rocks. The analogy between the Werra salt and fluid/melt bearing mineral aggregates is significant, because the GBS – assisted mechanisms are regarded as the most important for accommodation of strain in mineral aggregates (Langdon and Vastava, 1982; Zhang et al., 1994; Ranalli, 1995) although their understanding was so far obscured by the technical difficulties in reproducing the fluid/melt assisted GBS in the experiments (e.g. Rutter and Neumann, 1995; Gleason et al., 1999; Rosenberg and Handy, 2005; Rybacki et al., 2008). Fine-grained ultra-mylonites deformed by diffusion flow accommodated

GBS typical of extreme elongation of granular aggregates (e.g. Boullier and Gueguen, 1975; Schulmann et al., 2008b) could be produced by continuous grain dissection along cracks initiated from high stress concentration sites (grain boundary triple junctions, grain boundary ledges, solid or fluid inclusions). Comparably to the Werra rock salt, microcracking during GBS in rocks should take place around the lattice or grain boundary inhomogeneities such as solid (e.g. perthite exsolutions in feldspars) or fluid inclusions in grains or grain boundary ledges (Závada et al., 2007; Rybacki et al., 2010). Microcracking in aggregates deforming in the GBS regime can also explain the seismic events in the lower crust (White, 1996; Rybacki et al., 2010).

6. Conclusions

Intense deformation of the perennial fine-grained perennial Werra rock salt from the Neuhof mine was accommodated by coupled activity of solution-precipitation, grain boundary sliding and microcracking of halite grains. The intra-granular microcracks in the halite aggregate formed due to stress concentrations at fluid inclusion trail tips as Griffith tensional cracks or due to stress concentrations at grain boundary irregularities generated by grain boundary sliding. The same interfaces likely failed more than once during the identified coupled solution-precipitation—grain boundary sliding—microcracking creep. The role of high pore pressures and hydrofracturing for some of the cracks initiated from grain boundaries cannot be excluded. Transgranular microcracking promoted the activity of solution-precipitation creep by (1) grain-size decrease and (2) ingress of new brine into the grain boundary network, where the microcracks cross-cut the fluid inclusion trails within the sedimentary grain cores. In addition, new brine ingress into the grain boundary network is provided by, excavation of the fluid inclusion trail bearing cores by the non-conservative grain boundary migration. The identified interplay of mechanical (microcracking) and chemical (solution-precipitation, or diffusion flow in general) physical processes represents a concept that helps understanding the principles controlling the evolution of microstructure and rheology for silicate rocks deformed by diffusion flow deformation mechanisms coupled with grain boundary sliding.

Acknowledgments

This work was funded by a Portuguese scientific grant No.: PTDC/CTE-GIX/098696/2008, the Czech Science Foundation grant No.: 205/03/0204 and by the Deutsche Forschungsgemeinschaft (Project UR 64/9-2). Fruitful discussions with J. Cosgrove and L. Palatinus and a review by Colin Peach that improved the concept of this paper are acknowledged. We thank also to W. Krauss from GED institute at RWTH Aachen University for his help with preparing thin sections and Z. Schléder, who created the thin sections investigated in this study and the first figure, which was used from one of his earlier manuscripts. The authors would like to thank Tom G. Blenkinsop for the editorial handling.

References

Anthony, T., Cline, H.E., 1973. Thermomigration of liquid droplets in salt. In: Fourth Symposium on Salt.
Beer, W.W., 1996. Kalilagerstätten in Deutschland. Kali und Steinsalz 12 (Heft 1), 18–30.
Berest, P., Blum, P.A., Charpentier, J.P., Gharbi, H., Vales, F., 2005. Very slow creep tests on rock samples. International Journal of Rock Mechanics and Mining Sciences 42, 569–576.
Blenkinsop, T.G., 2000. Deformation Microstructures and Mechanisms in Minerals and Rocks. Springer, ISBN 9780412734809, 041273480X, 150 pp.
Boullier, A.M., Gueguen, Y., 1975. SP-mylonites – origin of some mylonites by superplastic flow. Contributions to Mineralogy and Petrology 50 (2), 93–104.
Čadek, J., 1988. Creep in Metallic Materials. Elsevier, Amsterdam, Netherlands, 372 pp.
Carter, N.L., Horseman, S.T., Russel, J.E., Handin, J., 1993. Rheology of rocksalt. Journal of Structural Geology 15, 1257–1271.
Celma, A.G., Donker, H., 1994. Radiation-induced creep of confined NaCl. Radiation Effects and Defects in Solids 132 (3), 223–247.
Celma, A.G., Donker, H., 1996. The Effect of Gamma Radiation in Salt. Technical report, EUR-Report 16743EN.
Chan, K.S., Munson, D.E., Bodner, S.R., Fossum, A.F., 1996. Cleavage and creep fracture of rock salt. Acta Materialia 44, 3553–3565.
Culshaw, N.G., Beaumont, C., Jamieson, R.A., 2006. The orogenic superstructure-infrastructure concept: revisited, quantified, and revived. Geology 34 (9), 733–736.
Daines, M.J., Kohlstedt, D.L., 1997. Influence of deformation on melt topology in peridotites. Journal of Geophysical Research, Solid Earth 102 (B5), 10257–10271.
Desbois, G., Urai, J.L., Kukla, P.A., Konstanty, J., Baerle, C., 2011a. High-resolution 3D fabric and porosity model in a tight gas sandstone reservoir: a new approach to investigate microstructures from mm- to nm-scale combining argon beam cross-sectioning and SEM imaging. Journal of Petroleum Science and Engineering 78, 243–257.
Desbois, G., Urai, J.L., Kukla, P.A., 2009. Morphology of the pore space in claystones – evidence from BIB/FIB ion beam sectioning and cryo-SEM observations. eEarth Discussion 4, 15–22.
Desbois, G., Urai, J.L., Kukla, P.A., Wollenberg, U., Pérez-Willard, F., Radí, Z., Sandor, R., 2011b. Distribution of brine in grain boundaries during static recrystallization in wet, synthetic halite: insight from Broad Ion Beam sectioning and SEM observation at cryogenic temperature. Contributions to Mineralogy and Petrology. doi:10.1007/s00410-011-0656-x (online first).
Desbois, G., Závada, P., Schléder, Z., Urai, J.L., 2010. Deformation and recrystallization mechanisms in actively extruding salt fountain: microstructural evidence for a switch in deformation mechanisms with increased availability of meteoric water and decreased grain size (Qum Kuh, central Iran). Journal of Structural Geology 32 (4), 580–594.
Drury, M., Urai, J., 1990. Deformation-related recrystallization processes. Tectonophysics 172, 235–253.
Ghoussoub, J., Leroy, Y.M., 2001. Solid-fluid phase transformation within grain boundaries during compaction by pressure solution. Journal of the Mechanics and Physics of Solids 49, 2385–2430.
Gleason, G.C., Bruce, V., Green, H.W., 1999. Experimental investigation of melt topology in partially molten quartzo-feldspathic aggregates under hydrostatic and non-hydrostatic stress. Journal of Metamorphic Geology 17 (6), 705–722.
Goldich, S.S., 1938. A study in rock-weathering. Journal of Geology 46, 17–58.
Griffith, A.A., 1921. The phenomena of rupture and flow in solids. Philosophical Transactions of the Royal Society of London, A 221, 163–198.
Handy, M.R., 1994. Flow laws for rocks containing 2 nonlinear viscous phases – a phenomenological approach. Journal of Structural Geology 16 (3), 287–301.
Hickman, S.H., Evans, B., 1991. Experimental pressure solution in halite: the effect of grain/interphase boundary structure. Journal of the Geological Society 148, 549–560.
Hirth, G., Kohlstedt, D.L., 1995. Experimental constraints on the dynamics of the partially molten upper-mantle – deformation in the diffusion creep regime. Journal of Geophysical Research, Solid Earth 100 (B2), 1981–2001.
Holdoway, K.A., 1973. Behavior of fluid inclusions in salt during heating and irradiation. In: Fourth Symposium on Salt.
Holtzman, B.K., Groebner, N.J., Zimmerman, M.E., Ginsberg, S.B., Kohlstedt, D.L., 2003. Stress-driven melt segregation in partially molten rocks. Geochemistry Geophysics Geosystems 4, 8607.
Hoppe, W., 1960. Die Kali- und Stensalzlagerstätten des Zechsteins in der Deutschen Demokratischen Republik. Teil 1: Das Werra- Gebiet. Freiberger Forsch.-H. C 97 (I), 166.
Hubbert, M.K., Rubey, W.W., 1959. Role of fluid pressure in mechanics of overthrust faulting. Geological Society of America Bulletin 70, 116–166.
Hudec, M., Jackson, M., 2007. Terra infirma: understanding salt tectonics. Earth-Science Reviews 82, 1–28.
Jackson, M.P.A., 1985. Natural Strain in Diapiric and Glacial Rocksalt, with Emphasis on Oakwood Dome, East Texas. Bureau of Economic Geology, The University of Texas at Austin, Texas.
Jaoul, O., Tullis, J., Kronenberg, A., 1984. The effect of varying water contents on the creep-behavior of Heavitree quartzite. Journal of Geophysical Research, Solid Earth 89 (NB6), 4298–4312.
Käding, K.C., Sessler, W., 1994. Befahrung Kalibergwerkes Neuhof-Ellers der Kali und Steinsalz AG bei Fulda (Exkursion am 8. April 1994). Jber Mitt. Oberrhein Geol. Ver. 76, 191–197.
Kassner, M.E., Hayes, T.A., 2003. Creep cavitation in metals. International Journal of Plasticity 19 (10), 1715–1748.
Kenis, I., Urai, J.L., van der Zee, W., Hilgers, C., Sintubin, M., 2005. Rheology of fine-grained siliciclastic rocks in the middle crust-evidence from structural and numerical analysis. Earth and Planetary Science Letters 233, 351–360.
Kozak, J., Sileny, J., Waniek, L., 1981. Laboratory investigations on fault plane induced tensile cracks. Studia Geophysica Et Geodaetica 25 (4), 332–342.
Kranz, R., 1983. Microcracks in rocks – a review. Tectonophysics 100 (1–3), 449–480.
Langdon, T.G., Vastava, R.B., 1982. An evaluation of deformation models for grain boundary sliding. In: Rohde, R.W., Swearengen, J.C. (Eds.), Mechanical Testing

for Deformation Model Development. Am. Soc. for Test. of Mater., Philadelphia, PA.
Langer, M., 1993. Use of solution-mined caverns in salt for oil and gas storage and toxic waste disposal in Germany. Engineering Geology 35, 183–190.
Leammlen, M., 1970. Geologische Karte von Hessen 1:25000 mit Erläuterungen. Blatt Nr. 5523. Neuhof, Wiesbaden, Germany.
Lehner, F., 1995. A model for intergranular pressure solution in open systems. Tectonophysics 245, 153–170.
Lexa, O., Štípská, P., Schulmann, K., Baratoux, L., Kröner, A., 2005. Contrasting textural record of two distinct metamorphic events of similar P-T conditions and different durations. Journal of Metamorphic Geology 23 (8), 649–666.
Littke, R., Bayer, U., Gajewski, D., Nelskamp, S. (Eds.), 2008. Dynamics of Complex Intracontinental Basins – The Central European Basin System. Springer-Verlag, Berlin-Heidelberg, ISBN 978-3-540-85084-7.
Lockhorst, A. (Ed.), 1998. NW European Gas Atlas-composition and Isotope Ratios of Natural Gases. GIS application on CD-ROM by the British Geological Survey Bundesanstalt für Geowissenschaften und Rohstoffe, Danmarks og Gronlands Geologiske, Undersogelse, Netherlands Instituut voor Toegepaste geowetenschappen, Panstwowy Instytut Geologiczny, European Union.
Lux, K.-H., 2005. Long-term behaviour of sealed liquid-filled salt cavities—a new approach for physical modelling and numerical simulation—basics from theory and lab investigations. Erdöl Erdgas Kohle 121, 414–422.
Mitra, G., 1978. Ductile deformation zones and mylonites: the mechanical processes involved in the deformation of crystalline basement rocks. American Journal of Science 278, 1057–1084.
Niemeijer, A., Marone, C., Elsworth, D., 2010. Frictional strength and strain weakening in simulated fault gouge: competition between geometrical weakening and chemical strengthening. Journal of Geophysical Research, Solid Earth 115, B10207.
Passchier, C., Trouw, R., 2005. Microtectonics, second ed. Springer, Berlin; New York, 366 pp.
Peach, C., Spiers, C., Trimby, P., 2001. Effect of confining pressure on dilatation, recrystallization, and flow of rock salt at 150 °C. Journal of Geophysical Research, Solid Earth 106, 13315–13328.
Peach, C., Spiers, C.J., 1996. Influence of crystal plastic deformation on dilatancy and permeability development in synthetic salt rock. Tectonophysics 256, 101–128.
Perry, K.F., 2005. Natural Gas storage industry experience and technology: potential application to CO_2 geological storage. In: Carbon Dioxide Capture for Storage in Deep Geologic Formations. Elsevier Science, Amsterdam, pp. 815–825.
Poirier, J.P., 1985. Creep of Crystals. Cambridge University Press, Cambridge, UK, 260 pp.
Popp, T., Kern, H., Schulze, O., 2001. Evolution of dilatancy and permeability in rock salt during hydrostatic compaction and triaxial deformation. Journal of Geophysical Research, Solid Earth 106, 4061–4078.
Price, N., Cosgrove, J.W., 1990. Analysis of Geological Structures. Cambridge University Press, Cambridge, UK, 502 pp.
Przibram, K., 1954. Irradiation colours in minerals. Endeavour 13 (49), 37–41.
Ramsay, J.G., 1980. Crack-seal mechanism of rock deformation. Nature 284 (5752), 135–139.
Ranalli, G., 1995. Rheology of the Earth. Chapmann and Hall, New York, 413 pp.
Renner, J., Evans, B., Hirth, G., 2000. On the theologically critical melt fraction. Earth and Planetary Science Letters 181 (4), 585–594.
Rosenberg, C.L., 2001. Deformation of partially molten granite: a review and comparison of experimental and natural case studies. International Journal of Earth Sciences 90 (1), 60–76.
Rosenberg, C.L., Handy, M.R., 2005. Experimental deformation of partially melted granite revisited: implications for the continental crust. Journal of Metamorphic Geology 23 (1), 19–28.
Roth, H., 1957. Befahrung des Kalisalzbergwerkes "Wintershall" der Gewerkschafft Wintershall in Heringen/Werra. Fortschr. Miner. 35 (1), 82–88.
Rowan, M.G., Jackson, M.P.A., Trudgill, B.D., 1999. Salt-related fault families and fault welds in the northern Gulf of Mexico. AAPG Bulletin 83 (9), 1454–1484.
Rutter, E.H., Neumann, D.H.K., 1995. Experimental deformation of partially molten westerly granite under fluid-absent conditions, with implications for the extraction of granitic magmas. Journal of Geophysical Research, Solid Earth 100 (B8), 15697–15715.
Rybacki, E., Wirth, R., Dresen, G., 2008. High-strain creep of feldspar rocks: implications for cavitation and ductile failure in the lower crust. Geophysical Research Letters 35 (4), L04304.
Rybacki, E., Wirth, R., Dresen, G., 2010. Superplasticity and ductile fracture of synthetic feldspar deformed to large strain. Journal of Geophysical Research, Solid Earth 115 (B08209).
Schenk, O., Urai, J.L., 2004. Microstructural evolution and grain boundary structure during static recrystallization in synthetic polycrystals of sodium chloride containing saturated brine. Contributions to Mineralogy and Petrology 146, 671–682.
Schenk, O., Urai, J.L., 2005. The migration of fluid-filled grain boundaries in recrystallizing synthetic bischofite: first results of in-situ high-pressure, high-temperature deformation experiments in transmitted light. Journal of Metamorphic Geology 23 (8), 695–709.
Schenk, O., Urai, J.L., Piazolo, S., 2006. Structure of grain boundaries in wet, synthetic polycrystalline, statically recrystallizing halite – evidence from cryo-SEM observations. Geofluids 6 (1), 93–104.
Schléder, Z., 2006. Deformation mechanisms of naturally deformed rocksalt, PhD thesis. RWTH Aachen, Aachen.
Schléder, Z., Urai, J.L., 2005. Microstructural evolution of deformation-modified primary halite from the Middle Triassic Rot Formation at Hengelo, The Netherlands. International Journal of Earth Sciences 94 (5–6), 941–955.
Schléder, Z., Urai, J., 2007. Deformation and recrystallization mechanisms in mylonitic shear zones in naturally deformed extrusive Eocene–Oligocene rocksalt from Eyvanekey plateau and Garmsar hills (central Iran). Journal of Structural Geology 29, 241–255.
Schléder, Z., Burliga, S., Urai, J.L., 2007. Dynamic and static recrystallization-related microstructures in halite samples from the Klodawa salt wall (central Poland) as revealed by gamma-irradiation. Neues Jahrbuch Fur Mineralogie-Abhandlungen 184 (1), 17–28.
Schléder, Z., Urai, J.L., Nollet, S., Hilgers, C., 2008. Solution-precipitation creep and fluid flow in halite: a case study of Zechstein (z1) rocksalt from Neuhof salt mine (Germany). International Journal of Earth Sciences 97 (5), 1045–1056.
Schmatz, J., Urai, J.L., 2010. The interaction of fluid inclusions and migrating grain boundaries in a rock analogue: deformation and annealing of polycrystalline camphor-ethanol mixtures. Journal of Metamorphic Geology 28 (1), 1–18.
Schoenherr, J., Schléderr, Z., Urai, J.L., Littke, R., Kukla, P.A., 2010. Deformation mechanisms of deeply buried and surface-piercing Late Pre-Cambrian to Early Cambrian Ara Salt from interior Oman. International Journal of Earth Sciences 99 (5), 1007–1025.
Schoenherr, L., Urai, L.L., Kukla, P.A., Littke, R., Schléder, Z., Larroque, J.M., Newall, M.J., Al-Abry, N., Al-Siyabi, H.A., Rawahi, Z., 2007. Limits to the sealing capacity of rock salt: a case study of the infra-Cambrian Ara Salt from the South Oman salt basin. AAPG Bulletin 91, 1541–1557.
Schulmann, K., Lexa, O., Stipska, P., Racek, M., Tajcmanova, L., Konopasek, J., Edel, J.B., Peschler, A., Lehmann, J., 2008a. Vertical extrusion and horizontal channel flow of orogenic lower crust: key exhumation mechanisms in large hot orogens? Journal of Metamorphic Geology 26 (2), 273–297.
Schulmann, K., Martelat, J.E., Ulrich, S., Lexa, O., Stipska, P., Becker, J.K., 2008b. Evolution of microstructure and melt topology in partially molten granitic mylonite: implications for rheology of felsic middle crust. Journal of Geophysical Research, Solid Earth 113 (B10), B10406.
Schulze, O., Popp, T., Kern, H., 2001. Development of damage and permeability in deforming rock salt. Engineering Geology 61, 163–180.
Spiers, C., Schutjens, P., Brzesowsky, R., Peach, C., Liezenberg, J., Zwart, H., 1990. Experimental determination of constitutive parameters governing creep of rocksalt by pressure solution. In: Knipe, R., Rutter, E. (Eds.), Deformation Mechanisms, Rheology and Tectonics. Geological Society Special Publication, vol. 54, pp. 215–227.
Talbot, C.J., 1998. Extrusions of Hormuz salt in Iran. In: Blundell, D.J., Scott, A.C. (Eds.), 1998. Lyell: The Past is the Key to the Present, vol. 143. Geological Society Special Publications, pp. 315–334.
Talbot, C.J., Aftabi, P., 2004. Geology and models of salt extrusion at Qum Kuh, central Iran. Journal of the Geological Society 161 (2), 321–334.
Talbot, C.J., Jackson, M.P.A., 1987. Internal kinematics of salt diapirs. AAPG Bulletin 71 (9), 1068–1093.
Ter Heege, J., De Bresser, J., Spiers, C., 2005. Rheological behaviour of synthetic rocksalt: the interplay between water, dynamic recrystallization and deformation mechanisms. Journal of Structural Geology 27, 948–963.
Tullis, J., Yund, R.A., 1991. Diffusion creep in feldspar aggregates – experimental-evidence. Journal of Structural Geology 13 (9), 987–1000.
Urai, J., Schléder, Z., Spiers, C., Kukla, P., 2008. Dynamics of Complex Intracontinental Basins: The Central European Basin System. In: Chapter Flow and Transport Properties of Salt Rocks, pp. 2–5.
Urai, J., Spiers, C., 2007. The effect of grain boundary water on deformation mechanism and rheology of rocksalt during long-term deformation. In: Wallner, M., Lux, K.-H., Minkley, W., Hardy, H. (Eds.), The Mechanical Behaviour of Salt – Understanding of THMC Processes in Salt. Taylor & Francis Group, pp. 149–158.
Urai, J., Spiers, C., Peach, C., Franssen, R., Liezenberg, J., 1987. Deformation mechanisms operating in naturally deformed halite rocks as deduced from microstructural investigations. Geologie en Mijnbouw 66, 165–176.
Urai, J., Spiers, C., Zwart, H., Lister, G., 1986. Weakening of rocksalt by water during long term creep. Nature 324, 554–557.
van Opbroek, G., den Hartog, H.W., 1985. Radiation damage of NaCl: dose rate effects. Journal of Physics C: Solid State Physics 18, 257–268.
Wenk, H.R., Armann, M., Burlini, L., Kunze, K., Bortolotti, M., 2009. Large strain shearing of halite: experimental and theoretical evidence for dynamic texture changes. Earth and Planetary Science Letters 280 (1–4), 205–210.
White, J.C., 1996. Transient discontinuities revisited: pseudotachylyte, plastic instability and the influence of low pore fluid pressure on deformation processes in the mid-crust. Journal of Structural Geology 18 (12), 1471–1477.
Závada, P., Schulmann, K., Konopásek, J., Ulrich, S., Lexa, O., 2007. Extreme ductility of feldspar aggregates – melt-enhanced grain boundary sliding and creep failure: rheological implications for felsic lower crust. Journal of Geophysical Research, Solid Earth 112 (B10), B10210.
Zhang, Y., Hobbs, B.E., Jessell, M.W., 1994. The effect of grain-boundary sliding on fabric development in polycrystalline aggregates. Journal of Structural Geology 16 (9), 1315–1325.